Chemical Geology
January 2022, Volume 588 Pages 120678 (14p.)
https://doi.org/10.1016/j.chemgeo.2021.120678
https://archimer.ifremer.fr/doc/00865/97717/

Towards a holistic sulfate-water-O2 triple oxygen isotope systematics

Killingsworth B. A. [1, 2, *], Cartigny P. [3], Hayles J. A. [4], Thomazo C. [5, 6], Sansjofre P. [2], Pasquier V [7], Lalonde S., V [2], Philippot P. [3, 8, 9]

[1] United States Geological Survey, MS 954 National Center, 12201 Sunrise Valley Dr., Reston, Virginia 20192, USA
[2] CNRS-UMR6538 Laboratoire Géosciences Océan, European Institute for Marine Studies, Université de Bretagne Occidentale, 29280 Plouzané, France
[3] Institut de Physique du Globe de Paris, Sorbonne-Paris Cité, UMR 7154, CNRS-Université Paris Diderot, 75005 Paris Cedex 05, France
[4] Jacobs-JETS, Astromaterials Research and Exploration Science, Johnson Space Center, NASA, Houston, TX 77058, USA
[5] UMR CNRS/uB 6282 Laboratoire Biogéosciences, Université de Bourgogne Franche-Comté, 6 Bd Gabriel, 21000 Dijon, France
[6] Institut Universitaire de France, 75005 Paris, France
[7] Department of Earth and Planetary Sciences, Weizmann Institute of Science, Rehovot 76100, Israel
[8] Géosciences Montpellier, CNRS-UMR 5243, Université de Montpellier, Montpellier Cedex 5, France
[9] Instituto de Astronomia, Geofísica e Ciências Atmosféricas, Universidade de São Paulo, Rua do Matão, 1226 - Cidade Universitária, 05508-090 São Paulo, Brazil

* Corresponding author : B. A. Killingsworth email address : bkillingsworth@usgs.gov

Abstract :

Triple oxygen isotope (Delta O-17 with delta O-18) signals of H2O and O-2 found in sulfate of oxidative weathering origin offer promising constraints on modern and ancient weathering, hydrology, atmospheric gas concentrations, and bioproductivity. However, interpretations of the sulfate-water-O-2 system rely on assuming fixed oxygen-isotope fractionations between sulfate and water, which, contrastingly, are shown to vary widely in sign and amplitude. Instead, here we anchor sulfate-water-O-2 triple oxygen isotope systematics on the homogeneous composition of atmospheric O(2)with empirical constraints and modeling. Our resulting framework does not require a priori assumptions of the O-2- versus H2O-oxygen ratio in sulfate and accounts for the signals of mass-dependent and mass-independent fractionation in the Delta O-17 and delta O-18 of sulfate's O-2-oxygen source. Within this framework, new Delta O-17 measurements of sulfate constrain similar to 2.3 Ga Paleoproterozoic gross primary productivity to between 6 and 160 times present-day levels, with important implications for the biological carbon cycle response to high CO2 concentrations prevalent on the early Earth.

Keywords : Sulfate, Oxygen isotopes, Atmospheric oxygen, Sulfide oxidation, Paleoclimate

1. INTRODUCTION

As a product of sulfide oxidation, sulfate results from sulfuric acid chemical weathering that increases acidity, alkalinity, and concentration of metals in mining environments (Raymond and Oh, 2009), while asserting controls on atmospheric O_2 and CO_2 over millions of years (Berner, 2006). Oxygen isotopes of sedimentary sulfates in rocks are ideal for understanding Earth's O_2 history, environmental conditions of sulfide oxidation, and the biological imprints of local and/or global (i.e., ocean) sulfur cycling (Bao, 2015). Our understanding of the oxygen sources of sulfide-derived sulfate relies on decades of chemical and isotopic studies (e.g., Lloyd, 1968; Taylor et al., 1984; Van Everdingen and Krouse, 1988; Balci et al., 2007; Tichomirowa and Junghans, 2009; Heidel and Tichomirowa, 2011; Kanzaki and Murakami, 2019), reviews of pyrite oxidation mechanisms (Williamson and Rimstidt, 1994; Rimstidt and Vaughan, 2003), and isotope systematics (e.g., Van Everdingen and Krouse, 1988; Van Stempvoort and Krouse, 1994; Taylor and Wheeler, 1994; Seal, 2003; Gomes and Johnston, 2017). Such substantial research efforts emphasize the complexity of sulfide oxidation in which seven electrons are transferred in total, one or two at a time, proceeding through intermediate sulfur species from an S(-I) to S(VI) oxidation state (Rimstidt and Vaughan, 2003). Sulfide-derived sulfate gains oxygen from sources such as ambient water and O_2, as in the pyrite oxidation reactions given by Taylor and Wheeler (1994),

$$FeS_2 + 7/2O_2 + H_2O \rightarrow Fe^{2+} + 2SO_4^{2-} + 2H^+ \quad (1)$$

$$FeS_2 + 14Fe^{3+} + 8H_2O \rightarrow 15Fe^{2+} + 2SO_4^{2-} + 16H^+ \quad (2).$$

These reactions imply that the product sulfate incorporates 87.5 % O_2-oxygen during reaction (1) and 100 % water-oxygen via oxidation with Fe^{3+} in reaction (2). In turn, the rate of reaction (2) is limited by the oxidation of Fe^{2+} to Fe^{3+} by O_2,

$$Fe^{2+} + 1/4O_2 + H^+ \rightarrow Fe^{3+} + 1/2H_2O \quad (3).$$

This suggests that O_2 is required to sustain pyrite oxidation, with the cumulative sulfate product containing oxygen atoms from both water and O_2 in proportion to the contributions of reactions (1) and (2). Despite their utility, the mass balance of these reactions does not match the sulfate oxygen isotope end members inferred from field and experimental data (Fig. 1), which should include oxygen isotope fractionation as well. Although the direct incorporation of O_2-oxygen into pyrite-derived sulfate has recently been challenged (Hemingway et al., 2020), pyrite oxidation experiments at low O_2 concentrations (Johnson et al., 2019; Kanzaki and Murakami, 2019) and analyses of weathered shales (Gu et al., 2020) have consistently shown the O_2-dependence of pyrite oxidation. Experiments and fieldwork have also highlighted the role of O_2 for setting sulfate triple oxygen isotope ($\Delta^{17}O$ and $\delta^{18}O$) compositions (Farquhar et al., 2008; Kohl and Bao, 2011; Killingsworth et al., 2018; Waldeck et al., 2019). Sulfate $\Delta^{17}O$, adding a dimension beyond $\delta^{18}O$, is a powerful tracer of isotopic signatures of atmospheric O_2 through time (e.g., Bao, 2015; Crockford et al., 2019). We also suggest that sulfates in rocks could allow characterization of potentially long-term variations, on the order of 100s of millions of years, of the oxygen isotope difference between seawater and atmospheric O_2, which is known as the Dole Effect (Dole, 1935; Morita, 1935). However, to fully assess $\Delta^{17}O$ and $\delta^{18}O$ of sulfate, outstanding issues must be addressed. Three key assumptions have been that 1) all of sulfate's negative $\Delta^{17}O$ signal is inherited from oxidation with atmospheric O_2 that, in turn,

ultimately reflects mass-independent photochemistry, 2) the proportion of O_2-oxygen in a given sulfate can be estimated, *a priori*, as being less than 25 %, and 3) oxygen-isotope systematics of sulfates are effectively constrained by consistent sulfate-water oxygen-isotope differences. The first assumption has been a useful approximation for examining relatively large negative $\Delta^{17}O$ (please see methods for isotope notation and the capital delta definition used here) anomalies in sulfate that extend as low as $\Delta^{17}O_{0.528} = -1.84$ ‰ (Bao et al., 2009). However, for considerations of smaller $\Delta^{17}O$ variations (e.g., between −0.3 ‰ to +0.3 ‰), mass-dependent triple oxygen isotope effects must be included in sulfate $\Delta^{17}O$-based models (Cao and Bao, 2021). For example, the ^{17}O-deficit in sulfate's atmospheric O_2 oxygen source is not solely due to mass independence, as it is largely attributable to mass-dependent reactions such as kinetic isotope effects during respiration that contribute to the Dole Effect (Luz et al., 2014; Young et al., 2014). The second assumption that places a maximum limit of 25 % for the fraction of O_2-oxygen in sulfates (e.g., Balci et al., 2007; Bao et al., 2008; Kohl and Bao, 2011; Crockford et al., 2019), may result in overestimations of the negative $\Delta^{17}O$ of O_2 that in turn affects constraints on ancient CO_2 and bioproductivity. Lastly, the third assumption anchors the oxygen isotope systematics of sulfate on fractionations between sulfate and water that are shown to be highly variable in sign and amplitude (see review in Gomes and Johnston, 2017). The isotopic relationships, and the isotopic constraints on the proportion of atmospheric O_2-oxygen in sulfate, are unconstrained because oxygen-isotope differences between sulfate and water are effectively moving targets. Oxygen of sulfate is predicted to carry a mix of equilibrium and non-equilibrium isotopic signatures that have been summarized, using available constraints, by Cao and Bao (2021). However, despite the leverage of isotopic

techniques, fixed magnitudes and signs for oxygen-isotope fractionations between sulfate and water (e.g., equations 13 and 15-18 in Cao and Bao, 2021) do not match sulfate results, either (Fig. 1). This mismatch between isotopic predictions and data is clearly observed with $\delta^{18}O$ even before introducing the added dimension of $\Delta^{17}O$. Considering these issues, outstanding assumptions need to be eliminated by updating sulfate-oxygen isotope systematics alongside an atmospheric O_2 triple oxygen isotope model that can handle both large and small $\delta^{18}O$ and $\Delta^{17}O$ variations.

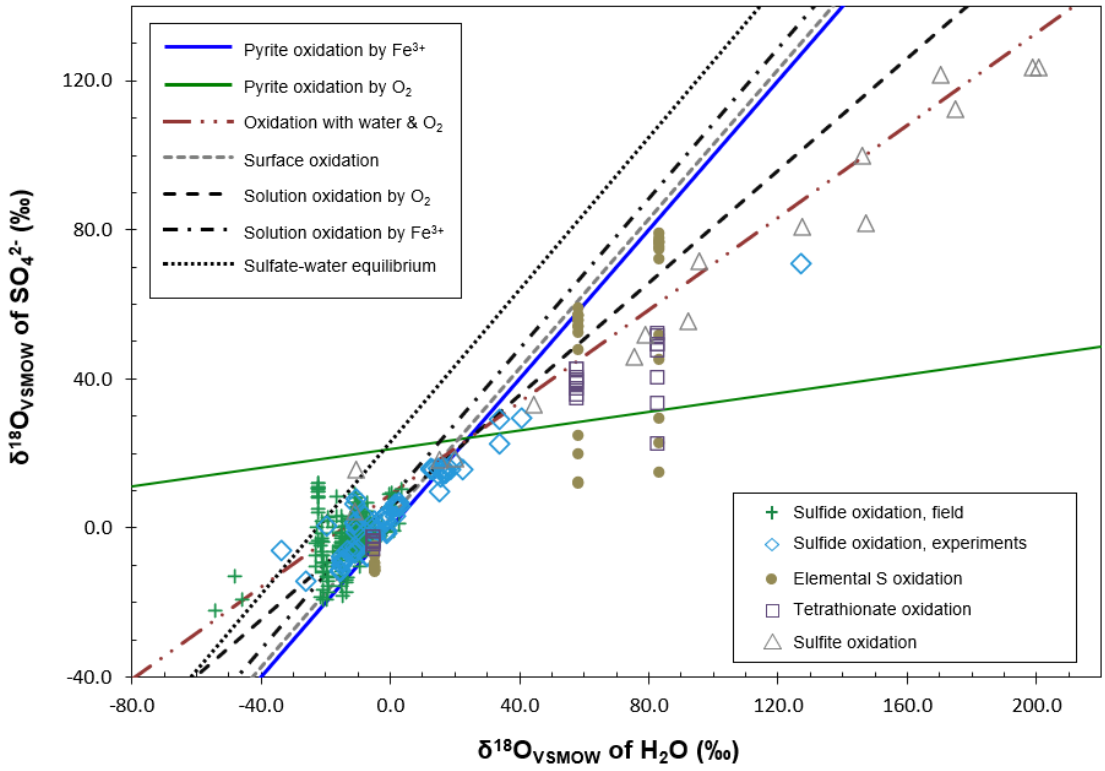

Figure 1. Paired sulfate and water oxygen isotope data with predicted curves for the sulfate-water-O_2 system from mass balance and isotopic approaches. The data are from original and compiled sources in Van Everdingen and Krouse, 1988; Seal, 2003; Balci et al., 2007; Kohl and Bao, 2011; Hendry et al., 1989; Sun et al., 2015; Pierre et al., 1984; Balci et al., 2017; and Krouse et al., 1991. The data are from field samples (crosses), sulfide oxidation experiments (open diamonds), sulfite oxidation experiments (open triangles),

tetrathionate oxidation experiments (open squares), and elemental sulfur oxidation (filled circles). The solid lines represent the mass balance of reactions given by Taylor and Wheeler (1994), as described in the main text for pyrite oxidation by O_2 (equation 1) and Fe^{3+} (equation 2), and the dashed-dotted line is for oxidation with water and O_2 described in Van Stempvoort and Krouse (1994). The dashed lines show oxygen isotope fractionations for sulfate in the sulfate-water-O_2 system that are summarized and calculated in Cao and Bao (2021).

2. METHODS

2.1. METHODS: TRIPLE OXYGEN ISOTOPE NOTATION

Oxygen isotope data are reported in delta notation in units × 1000 ‰ as deviations from the international isotope standard Vienna Standard Mean Ocean Water (VSMOW), as

$$\delta \equiv R_{\text{sample}}/R_{\text{standard}} - 1 \qquad (4),$$

with R being the $^{18}O/^{16}O$ or $^{17}O/^{16}O$ isotope atomic ratio. We report oxygen-17 in linear capital delta notation, also in ‰, as

$$\Delta^{17}O \equiv \delta^{17}O - C \times \delta^{18}O \qquad (5),$$

where C is a reference slope of 0.528 useful for comparisons against meteoric waters and within low-temperature systems (e.g., Luz and Barkan, 2010). Our use of linear delta definitions helps characterize source-mixing because such mixing follows straight-line paths in multiple-isotope space. In contrast, under linear delta definitions, isotopic fractionation processes follow curved arrays. Model calculations use the logarithmic $\delta'^{1x}O$ and $\Delta'^{17}O$ delta definitions where appropriate. The $\Delta'^{17}O$ capital delta definition (Bao et al., 2016 and references therein) is

$$\Delta'^{17}O \equiv \delta'^{17}O - C \times \delta'^{18}O \qquad (6),$$

with δ' being a logarithmic definition of delta that is

$$\delta'^{1x}O = \ln(\delta^{1x}O + 1) = \ln(R_{\text{sample}}/R_{\text{standard}}) \qquad (7),$$

with ^{1x}O referring to the isotope ^{18}O or ^{17}O. The $\Delta^{17}O$ and $\Delta'^{17}O$ data are reported with respect to VSMOW when possible. For consistency and ease of comparison, we most frequently use the notation $\Delta^{17}O$. Between two given substances, two-isotope fractionation, such as between ^{16}O and ^{18}O, is commonly represented as $\alpha_{A\text{-}B} \equiv R_A/R_B$ and $\ln(\alpha_{A\text{-}B}) \equiv \delta'^{xx}O_A - \delta'^{xx}O_B$, with R_X representing the isotopic ratio, and $\delta'^{xx}O_X$ representing the isotopic delta of a sample A or B. However, given the contributions of multiple reservoirs of oxygen, each with specific fractionation factors between them (α), we instead use $\Delta\Delta^{17}O_{A\text{-}B}$ and $\Delta\delta^{18}O_{A\text{-}B}$ (Bao et al., 2016) to generically describe $\Delta^{17}O$ or $\delta^{18}O$ isotopic differences between two substances A and B. This convention also avoids the potential confusion when a single big delta is being used to describe isotopic differences (e.g., a two-isotope $\Delta^{18}O_{A/B}$ or $\Delta^{17}O_{A/B}$, after Coplen, 2011) at the same time as the three-isotope capital delta ($\Delta^{17}O$) is in use to describe triple oxygen isotope deviations from a reference slope *C*.

2.2. METHODS: THE ORIGIN OF THE TRIPLE OXYGEN ISOTOPE TRACERS FROM ATMOSPHERIC O_2 AND H_2O THAT ARE FOUND IN SULFATE

Most terrestrial processes fractionate oxygen isotopes according to differences in isotopic masses. These mass-dependent processes are largely predictable, within ±0.3 ‰ (e.g., for equilibrium processes, Hayles et al., 2017), of the terrestrial fractionation line at $\Delta^{17}O \approx \delta^{17}O - 1/2 \times \delta^{18}O$ (Thiemens, 2006; Figure 2 inset). In contrast, mass-independent signals in the terrestrial oxygen isotope system result from photochemical fractionations in the stratosphere that are characterized by the relationship $\delta^{17}O \approx \delta^{18}O$ (Thiemens and Heidenreich, 1983). A synthesis of isotope results from atmospheric species (Thiemens, 2006; Figure 2 inset) indicates stratospheric ozone has the largest mass-independent ^{17}O

enrichment ($\Delta^{17}O_{0.528} \approx +37$ ‰) while stratospheric CO_2 has a smaller ^{17}O enrichment ($\Delta^{17}O_{0.528} \approx +5$ ‰) ultimately derived from ozone. Meanwhile, tropospheric O_2 measurements ($\Delta^{17}O_{0.528} = -0.49$ ‰; Pack et al., 2017) indicate the ^{17}O-depleted balance is hosted by O_2 within the stratospheric network with relative reservoir sizes $O_2 > CO_2 > O_3$.

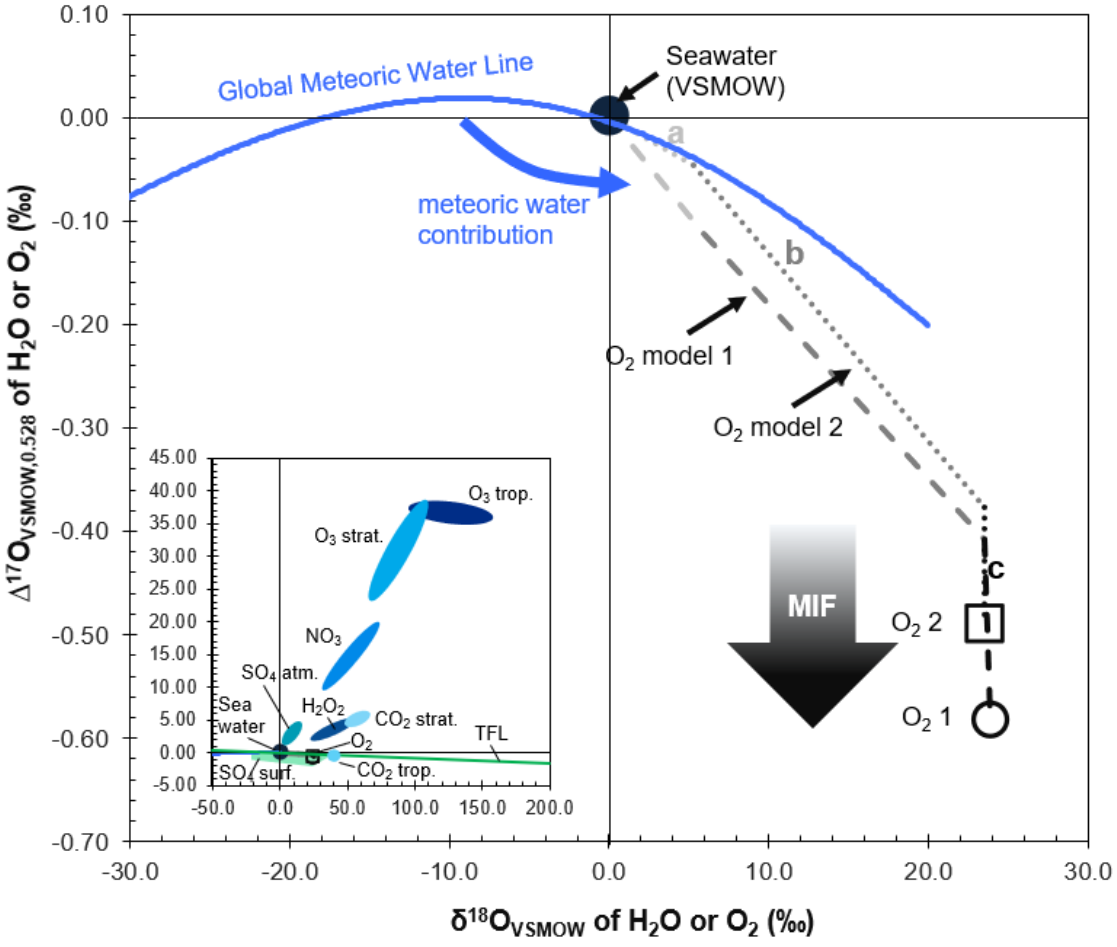

Figure 2. Simplified versions of two models of the oxygen isotopic differences between seawater and atmospheric O_2, or the Dole Effect, are shown alongside the triple oxygen isotope fractionation among meteoric waters, the Global Meteoric Water Line (a polynomial curve fit from Sengupta et al., 2020). The mass independently fractioned contribution from stratospheric reactions to the $\Delta^{17}O$ of O_2 is denoted with the arrow

labeled MIF. Model 1 and its respective O_2 composition (O_2 1) are from Luz et al. (2014), and model 2 and its respective O_2 (O_2 2) are from Young et al. (2014). The net fractionating processes contributing to final composition of atmospheric O_2 are lettered in sequence: the composition of seawater (represented by the isotope standard VSMOW) is found at the origin, which is the starting source of oxygen for meteoric waters, with both water sources contributing to (a) the photosynthetic production of O_2, followed by (b) effects of respiration on O_2, and (c) the stratospheric photochemical effect on O_2. The figure inset gives an expanded view of atmospheric oxygen-bearing species after the $\delta^{17}O$-$\delta^{18}O$ figure 6 in Thiemens (2006) that is redrawn here in $\Delta^{17}O$-$\delta^{18}O$. The abbreviations used for the figure inset labels are for tropospheric (trop.), stratospheric (strat.), atmospheric (atm.), and surficial (surf.).

Mass-dependent processes, such as within the hydrosphere, yield roughly predictable isotopic fractionations that have small but measurable variations that can be diagnostic. Starting with seawater at the origin, meteoric waters follow $\Delta^{17}O$-$\delta^{18}O$ trends that are indicated by a best-fit polynomial line, the Global Meteoric Water Line, in Figure 2. Given that meteoric water isotope compositions relate to both equilibrium and kinetic isotope effects whose mechanisms are dependent on temperature and relative humidity (e.g., Luz and Barkan, 2010), respectively, the isotopic relationships of waters are unlikely to have changed much over time. A different oxygen-isotope composition of seawater in the past would, however, require a shift in the anchor point for the oxygen isotope system of water, away from its current seawater origin defined by modern ocean water (VSMOW). Despite this possibility, the extant chert oxygen isotope record through the Proterozoic to the present does not require secular changes in ocean oxygen isotope composition (e.g., Sengupta et al., 2020).

The terrestrial Dole Effect (DE) was originally defined as the $\delta^{18}O$ difference (or $\Delta\delta^{18}O$) between tropospheric O_2 and seawater (Dole, 1935; Morita, 1935), which was further extended to $\Delta^{17}O$ (or $\Delta\Delta^{17}O_{tropO2-seawater}$) (Bender et al., 1994; Luz et al., 1999).

Parameterizations by Luz et al. (2014) and Young et al. (2014) generally agree that the modern Dole Effect is $\Delta\delta^{18}O_{tropO2-seawater} \approx +24$ ‰ as a consequence of photosynthetic O_2 of marine and terrestrial origin ($\Delta\delta^{18}O_{photoO2-seawater} \approx +6$ ‰) undergoing partial respiration by various organisms ($\Delta\delta^{18}O_{respiration-photoO2} \approx +18$ ‰); their extension to $\Delta^{17}O$ agrees in that the DE is $\Delta\Delta^{17}O_{tropO2-seawater} = -0.49$ ‰ to -0.58 ‰ reflecting photosynthetic O_2 ($\Delta\Delta^{17}O_{photoO2-seawater} = -0.04$ ‰ to -0.1 ‰) being partially respired ($\Delta\Delta^{17}O_{respiration-photoO2} = -0.3$‰) with a further ^{17}O deficit from mixing with mass independently fractionated stratospheric O_2 ($\Delta\Delta^{17}O_{tropO2-respiredphotoO2} = -0.1$ ‰ to -0.18 ‰) (Fig. 2). Stratospheric O_2 with extraordinary ^{17}O depletion, because of low-O_2 conditions and/or a balance with high CO_2, is considered responsible for the most negative $\Delta^{17}O$ found in ancient sulfates from rocks (e.g., Bao et al., 2009; Crockford et al., 2018).

Modeling of the response of $\Delta^{17}O_{tropO2}$ to high CO_2 during the ~635 Ma Marinoan ^{17}O-depletion event (Cao and Bao, 2013) opened the doors to further inquiry of sulfate's $\Delta^{17}O$ tracer of O_2 (e.g., Hodgkiss et al., 2019; Planavsky et al., 2020). However, the Dole Effect (Luz et al., 2014; Young et al., 2014) has yet to be integrated into a model that is tailored to multi-million-year timescales which can separately account for mass-independent photochemistry, mass-dependent biological fractionation of O_2, and calculation of the full triple oxygen isotope composition of O_2 ($\Delta^{17}O$ *and* $\delta^{18}O$) that is all ground-truthed by sulfate triple oxygen isotope constraints on O_2 from the rock record. Therefore, our O_2 model is done in concert with a critical reassessment of sulfate-water-O_2 oxygen isotope systematics.

2.3. METHODS: MODEL CALCULATIONS

As done with earlier approaches, sulfate-constrained triple oxygen isotope composition of O_2 can be used for inverted model solutions of pCO_2 (e.g., Bao et al., 2008), pO_2 (e.g., Planavsky et al., 2020), or bioproductivity (e.g., Crockford et al., 2018). We start with the $\Delta^{17}O_{O2}$ box model of Cao and Bao (2013) that forms the basis for the sulfate-constrained $\Delta^{17}O_{O2}$ models that followed it. We re-calibrate that original model with partitioning of O_2-oxygen isotope signals coming from stratospheric reactions versus biological contributions of O_2 and solve for $\delta^{18}O_{O2}$, both features which were lacking in the original model. This is followed by a detailed calculation of the biological contribution to atmospheric O_2 for completeness as a check on the isotopic implications of separating or combining land and marine contributions (note that only the marine contribution was considered in Cao and Bao (2013)). Further, this allows isolation of 2nd- and 3rd-order biological controls such as photosynthetic O_2 flux and respiration. Although useful for further examination, as constructed, the detailed biological O_2 model (*bioO2mod*) is not used in our final simplified O_2 model because the O-isotope composition of biological O_2 is taken as a constant, as detailed further below. Thus, the final applied model is simple in that it assumes the biological contribution has a fixed oxygen isotope composition. The ratios of the flux of stratospheric O_2 versus total O_2 and steady state O_2 versus stratospheric O_2 within the stratosphere O_2-CO_2-O_3 are also fixed. Meanwhile, pO_2, pCO_2, O_2 residence time, and the flux of oxygen production are allowed to vary within additional constraints imposed from literature sources. After Crockford et al. (2018), the flux of oxygen production is considered stoichiometrically related to photosynthetic oxygen flux, which, in turn, is proportional to gross primary productivity (GPP). Because of the assumption that the ratio

of GPP to respiration is fixed, GPP could also be a stand-in for net primary production that is equal to GPP minus respiration. This is built into the model due to the assumption that the biological contribution has a fixed O-isotope composition with a majority of the isotopic signature being due to respiration. We will further test the assumption that the ratio of GPP/respiration is fixed within the model. Although our model is a refinement, it is still only a rough approximation due to the many uncertainties about the past biosphere, pCO_2, and pO_2. As such, we will test the model's applicability by comparing with existing O-isotope records of sulfate. Then, specifically in the case of ca. ~2.3 Ga Kazput barite analyzed for its $\Delta^{17}O$ as part of this study, we will leverage $\Delta^{17}O_{barite}$ and $\delta^{18}O_{barite}$ measurements to estimate the triple oxygen isotope composition of O_2, then, ranges of pCO_2 and pO_2 at ~2.3 Ga will be taken from published geochemical proxy or model constraints to invert the model and solve for GPP.

In sum, here the improvements with respect to the Cao and Bao (2013) model are that we can solve for $\delta^{18}O_{O2}$, and the stratospheric mass-independent and biological mass-dependent contributions are separated. The updated model is accordingly retuned to solve for the isotopic composition of modern O_2. This retuning is crucial to ensure the model works under known constraints before applying it to ancient records where pO_2 and pCO_2 are poorly constrained. Three aspects are first examined separately and then integrated into the final model as follows, 1) the stratospheric photochemical effect (*strateff*) on tropospheric O_2 is isolated and calculated, 2) the stratospheric effect module (*strateffmod*) is retuned for the final model, 3) the module for the effect of the biosphere on atmospheric O_2 (*bioO2mod*) is constructed, and 4) the final model (*tropO2*) returns the triple oxygen

isotope composition ($\delta^{18}O$ and $\Delta^{17}O$) of tropospheric O_2 as a function of pO_2, pCO_2, and marine and terrestrial biological O_2 production.

The photochemical effect that we term *strateff* is the diminution of the tropospheric O_2 triple oxygen isotope composition, i.e., the lowering of its ^{17}O and ^{18}O versus ^{16}O, by mixing with O_2 that has been isotopically fractionated in the stratosphere. Separate calculation of the *strateff* must be done to distinguish the mass independent effect from the mass dependent effects (from the biosphere) on the composition of atmospheric O_2. Note that the *strateff* is due to the nearly equal enrichment of ^{17}O and ^{18}O (versus ^{16}O) in photochemically reacted ozone (O_3) from which electronically excited atomic oxygen goes on to react and enrich CO_2 in ^{17}O and ^{18}O (Yung et al., 1991). This is balanced by the depletion of ^{17}O and ^{18}O in the O_2 that is the ultimate source of ozone (Wen and Thiemens, 1993). By isotopic mass balance, the large tropospheric O_2 reservoir has a small depletion of ^{17}O and ^{18}O compared to the larger enrichments of the ^{17}O and ^{18}O in the much smaller O_3 and CO_2 reservoirs. The stratospheric effect on tropospheric O_2 was calculated by Bender et al. (1994) as a −0.4 ‰ decrease in both $\delta^{17}O_{O2}$ and $\delta^{18}O_{O2}$. Later, the stratospheric effect on atmospheric O_2 was measured and calculated to be $\delta^{17}O = \delta^{18}O =$ −0.3 ±0.1 ‰ (Luz et al., 1999; Luz et al., 2014). We update the isotopic mass balance calculation (Bender et al., 1994) for incorporation into our model, as follows,

$$\delta^{1x}O_{strateff} = str\text{-}trp_{CO2} \times (pCO_2/pO_2) \times (\tau_{trpO2}/\tau_{trp\text{-}strO2}) \times -1 \qquad (8).$$

Descriptions of equation (8) parameters are found in Table 1, whereas $\delta^{1x}O_{strateff}$ is for both ^{17}O and ^{18}O. We calculate the *strateff* to be $\delta^{17}O_{strateff} = \delta^{18}O_{strateff} = -0.3648$ ‰, identical, within uncertainty, to the estimation by Luz et al. (1999, 2014).

Table 1
strateff

Parameter	description	value	unit or term	reference
$str\text{-}trp_{CO2}$	average $\delta^{18}O$ difference of stratospheric CO_2 versus tropospheric CO_2	8.0167	‰	Thiemens et al., 1995; Thiemens et al., 1991
pCO_2	partial pressure of CO_2 by volume	375	ppm	Cao and Bao, 2013
pO_2	partial pressure of O_2 by volume	209500	ppm	Cao and Bao, 2013
τ_{trpO2}	trop O_2 residence time in years	1271	yr	calculated in *strateffmod*
$\tau_{trp\text{-}strO2}$	trop O_2 turnover time in stratosphere in years	50	yr	Andrews et al., 2001
	sign change for O_2	−1		Bender et al., 1994

Next, we use the calculated *strateff* as constraint on the inverse module *strateffmod*, which will then match the triple oxygen isotope contributions to O_2 from the biosphere and stratosphere, today, and interface this constraint with the final model. Compared with the Cao and Bao (2013) model, the *strateffmod* now includes the biological flux of terrestrial photosynthetic O_2, not only marine photosynthetic O_2, and retunes the θ parameter, which is the fraction of steady state O_2 within the O_2-CO_2-O_3 reaction network versus total stratospheric O_2. As before, the θ parameter is tuned so that the model returns the isotopic composition of modern atmospheric O_2. However, now the biosphere's contribution to the ^{17}O depletion in tropospheric O_2 is separately accounted for. The *strateffmod* is calculated as follows, where $\delta^{1x}O$ refers to separate calculations for both $\delta^{17}O$ and $\delta^{18}O$, with parameters described in Table 2:

$$\delta^{1x}O_{strateffmod} = (-\delta^{1x}O_{CO2\text{-}O2} \times \gamma \times \theta \times \tau_{trpO2}) \div (1 + \rho + \gamma \times \theta \times \tau_{trpO2}) \qquad (9).$$

The *strateffmod* returns $\delta^{18}O_{strateffmod} = -0.3648$ ‰ and $\delta^{17}O_{strateffmod} = -0.3611$ ‰, and therefore $\Delta\Delta^{17}O_{tropO2-respiredphotoO2,0.528} = -0.1685$ ‰ for the stratospheric effect on modern tropospheric O_2.

Table 2
Parameters for calculation in eq. (9) of the *strateffmod*, the photochemical isotopic effect on tropospheric O_2 updated for incorporation into our final model.

Parameter	description	value	unit or term	Reference
F_{op}	flux of ocean oxygen production	1.09×10^{16}	mol/yr	Blunier et al., 2002
F_{lp}	flux of land oxygen production	1.90×10^{16}	mol/yr	Blunier et al., 2002
γ	ratio of stratospheric O_2 flux involved in stratosphere-troposphere gas exchange / total O_2	0.1321		Cao and Bao, 2013
θ	ratio of steady state O_2 within O_2-CO_2-O_3 reaction network / stratospheric O_2 (tuned)	0.00836		this study
ρ		pCO_2/pO_2		Shaheen et al., 2007
$\delta^{18}O_{CO2\text{-}O2}$	steady-state $\delta^{18}O_{CO2}$ normalized against $\delta^{18}O_{O2}$, within the O_2-CO_2-O_3 reaction network	$(64 + 146 \times \rho/1.23)/(1 + \rho/1.23)$	‰	Shaheen et al., 2007; Cao and Bao, 2013
$\delta^{17}O_{CO2\text{-}O2}$	as above, but for $\delta^{17}O_{CO2}$ versus $\delta^{17}O_{O2}$	$1.039 \times \delta^{18}O_{CO2\text{-}O2} - 7.1738$	‰	Cao and Bao, 2013
pCO_2	partial pressure of CO_2 by volume	375	ppm	Cao and Bao, 2013
pO_2	partial pressure of O_2 by volume	209500	ppm	Cao and Bao, 2013
O_{2trp}	tropospheric O_2 in moles	3.8×10^{19}	mol	Young et al., 2014
τ_{trpO2}	trop O_2 residence time in years	$O_{2trp} / (F_{op} + F_{lp})$	yr	

Our initial *strateffmod* state at modern conditions compares to the previous model (Cao and Bao, 2013) with a biosphere flux of O_2 that is more than doubled due to the inclusion of land production alongside marine production and a value of θ that is half of the previously used value. Note that θ is used here to be consistent with the Cao and Bao model but it is not to be confused with isotopic θ (see Table 2). The immediate implication is that, here, the contribution of stratospheric photochemistry to the negative $\Delta^{17}O$ of tropospheric O_2 is half of what it was in the Cao and Bao model, at least for the initial tuning to modern conditions. The important feature of the *strateffmod* for the final model is that it responds to variations in atmospheric pO_2 and pCO_2, after Cao and Bao (2013) and as based on the experimental results of Shaheen et al. (2007).

The next step after isolating the mass independent stratospheric effect is to characterize the triple oxygen isotope composition of biologically produced and respired O_2 in the *bioO2mod* model component, which accounts for the mass dependent effects on the triple oxygen isotope composition of O_2. Biologically affected O_2 is already constrained by the isotopic composition of modern atmospheric O_2 minus that of the stratospheric effect; therefore, the *bioO2mod* component is not used in the simplified version of the final model. Biological O_2 is combined from separate calculations of the Dole Effect coming from the marine and terrestrial biosphere, where their respective O_2 fluxes are F_{op} (ocean production) and F_{lp} (land production) (Blunier et al., 2002), and the triple oxygen isotope calculations are done separately for their respective $\delta^{17}O$ and $\delta^{18}O$ values (Luz et al., 2014) using known constraints summarized in Table 3. What emerges in our calculation is that the $\delta^{17}O$ and $\delta^{18}O$ of the present-day marine and terrestrial Dole Effect are within 0.3 ‰ of each other, a small range consistent with both prior work (Luz et al., 2014), and the relatively restricted long-term variations of the DE in ice core records (Yan et al., 2019). Another important aspect is that the large uncertainty for the global average oxygen isotope composition of global leaf water, for example $\delta^{18}O = 6.5 \pm 2.1$ ‰ (West et al., 2008), makes it necessary to adjust the $\delta^{17}O$ and $\delta^{18}O$ of leaf water in our model, similarly as Young et al., (2014), to match the biological O_2 to its final composition that is constrained by the *strateff*. Accordingly, our leaf water is $\delta^{18}O_{lw} = 7.69$ ‰ and $\delta^{17}O_{lw} = 4.03$ ‰. Because respiration effects are the most significant biological controls on the isotope composition of biological O_2, more refined triple oxygen isotope slopes (e.g. Ash et al., 2020) will be needed to examine smaller $\Delta^{17}O$-$\delta^{18}O$ variations of O_2 such as found in ice cores. The summed marine and terrestrial biological O_2 composition is constrained by $\delta^{18}O_{O2modern}$ =

24.15 ‰ and $\delta^{17}O_{O2modern}$ = 12.26 ‰ ($\Delta^{17}O_{0.528}$ = −0.49 ‰) (Pack et al., 2017), and the *strateffmod* results, making it

$$\delta^{1x}O_{bioO2} = \delta^{1x}O_{O2modern} - \delta^{1x}O_{strateffmod} \quad (10),$$

whereas it is 24.51 ‰ for $\delta^{18}O_{bioO2}$ and = 12.62 ‰ for $\delta^{17}O_{bioO2}$, with $\Delta^{17}O_{0.528}$ = −0.32 ‰, for the total contribution of the biosphere to the DE of O_2. The $\delta^{17}O_{bioO2mod}$ and $\delta^{18}O_{bioO2mod}$ are calculated as

$$\delta^{1x}O_{bioO2mod} = x_m \times \delta^{1x}O_{mDE} + x_t \times \delta^{1x}O_{tDE} \quad (11).$$

Table 3
Parameters and expressions for calculation in eq. (11) of the *bioO2mod*, the oxygen isotope effect from the biosphere on tropospheric O_2.

Parameter	description	value	unit or term	reference
x_m	fraction of marine production	$F_{op}/(F_{op} + F_{lp})$		
x_t	fraction of terrestrial production	$F_{lp}/(F_{op} + F_{lp})$		
$\delta^{17}O_{mpo}$	$\delta^{17}O$ of marine photosynthetic oxygen	(e^($\delta'^{17}O_{mpo}$/1000)-1) × 1000	‰	
$\delta^{18}O_{mpo}$	$\delta^{18}O$ of marine photosynthetic oxygen	5.00	‰	Luz et al., 2014
$\delta'^{17}O_{mpo}$		0.521 × $\delta'^{18}O_{mpo}$	‰	Luz et al., 2014 for beta = 0.521
$\delta'^{18}O_{mpo}$		ln($\delta^{18}O_{mpo}$/1000 + 1) × 1000	‰	
$\delta^{17}O_{mresp}$	$\delta^{17}O$ of marine respiration	(e^($\delta'^{17}O_{mresp}$/1000) − 1) × 1000	‰	
$\delta^{18}O_{mresp}$	$\delta^{18}O$ of marine respiration	24.3 − $\delta^{18}O_{mpo}$	‰	calculated from Luz et al., 2014
$\delta'^{17}O_{mresp}$		0.516 × $\delta'^{18}O_{resp}$	‰	Luz et al., 2014 beta 0.516
$\delta'^{18}O_{mresp}$		ln($\delta^{18}O_{mresp}$/1000 + 1) × 1000	‰	
$\delta^{17}O_{mDE}$	$\delta^{17}O$ of marine Dole Effect	$\delta^{17}O_{mpo}$ + $\delta^{17}O_{mresp}$	‰	
$\delta^{18}O_{mDE}$	$\delta^{18}O$ of marine Dole Effect	$\delta^{18}O_{mpo}$ + $\delta^{18}O_{mresp}$	‰	
$\delta'^{17}O_{mDE}$		ln($\delta^{17}O_{mDE}$/1000 + 1) × 1000	‰	
$\delta'^{18}O_{mDE}$		ln($\delta^{18}O_{mDE}$/1000 + 1) × 1000	‰	
$\delta^{17}O_{lw}$	leaf water $\delta^{17}O$ tuned so that $\delta^{17}O_{O2modern} - \delta^{17}O_{strateffmod} = \delta^{17}O_{bioO2}$	4.0280	‰	this study
$\delta^{18}O_{lw}$	leaf water $\delta^{18}O$ tuned so that $\delta^{18}O_{O2modern} - \delta^{18}O_{strateffmod} = \delta^{18}O_{bioO2}$	7.6878	‰	this study
$\delta'^{17}O_{lw}$		ln($\delta^{17}O_{lw}$/1000+1) × 1000	‰	
$\delta'^{18}O_{lw}$		ln($\delta^{18}O_{lw}$/1000+1) × 1000	‰	
$\delta^{17}O_{eqdo}$	$\delta^{17}O$ of equilibrium isotope fractionation of dissolved O_2 with respect to atmospheric O_2	(e^($\delta'^{17}O_{eqdo}$/1000)-1) × 1000	‰	
$\delta^{18}O_{eqdo}$	$\delta^{18}O$ of equilibrium isotope fractionation of dissolved O_2 with respect to atmospheric O_2	0.75	‰	Luz et al., 2014
$\delta'^{17}O_{eqdo}$		0.5284 × $\delta'^{18}O_{eqdo}$	‰	Blunier et al., 2002 for beta = 0.5284

$\delta'^{18}O_{eqdo}$		$\ln(\delta^{18}O_{eqdo}/1000+1) \times 1000$	‰	
$\delta^{17}O_{tresp}$	$\delta^{17}O$ of terrestrial respiration	$(e^{\wedge}(\delta'^{17}O_{tresp}/1000)-1) \times 1000$	‰	
$\delta^{18}O_{tresp}$	$\delta^{18}O$ of terrestrial respiration	17.7	‰	Landais et al., 2007; Luz et al., 2014
$\delta'^{17}O_{tresp}$		$0.514 \times \delta'^{18}O_{tresp}$	‰	Luz et al., 2014 for beta = 0.514
$\delta'^{18}O_{tresp}$		$\ln(\delta^{18}O_{tresp}/1000+1) \times 1000$	‰	
$\delta^{17}O_{tDE}$	$\delta^{17}O$ of the terrestrial DE	$\delta^{17}O_{lw}+\delta^{17}O_{tresp}-\delta^{17}O_{eqdo}$	‰	calculation after Luz et al., 2014
$\delta^{18}O_{tDE}$	$\delta^{18}O$ of the terrestrial DE	$\delta^{18}O_{lw}+\delta^{18}O_{tresp}-\delta^{18}O_{eqdo}$	‰	calculation after Luz et al., 2014
$\delta'^{17}O_{tDE}$		$\ln(\delta^{17}O_{tDE}/1000+1) \times 1000$	‰	
$\delta^{17}O_{O2modern}$		12.26	‰	Pack et al., 2017
$\delta^{18}O_{O2modern}$		24.15	‰	Pack et al., 2017

Our final simplified model, *tropO2*, gives the full triple oxygen isotope composition of tropospheric O_2, separately for $\delta^{17}O_{tropO2}$ and $\delta^{18}O_{tropO2}$ from which $\Delta^{17}O$ can be calculated, as a function of the fluxes of photosynthetic O_2 from the land and ocean biospheres, and the partial pressures of O_2 and CO_2, as integrated in the previously described modules:

$$\delta^{1x}O_{tropO2} = \delta^{1x}O_{strateffmod} + \delta^{1x}O_{bioO2mod} \quad (12).$$

In the simplified model, the fixed $\delta^{17}O_{bioO2}$ and $\delta^{18}O_{bioO2}$ calculated from equation (10) are used within equation (12) instead of $\delta^{17}O_{bioO2mod}$ and $\delta^{18}O_{bioO2mod}$. If constraints on the isotope composition of tropospheric O_2, pO_2, and pCO_2 are available then the model can be inverted to solve for GPP (as equivalent to the sum of oxygen production in the ocean and on land). The interpretation $\Delta^{17}O$ and $\delta^{18}O$ measurements of sulfate within our updated sulfate-water-O_2 framework will allow for estimation of the $\Delta^{17}O$ and $\delta^{18}O$ of tropospheric O_2. To do this requires calculating between the triple oxygen isotope compositions of sulfate, O_2^* for the fractionated O_2-oxygen incorporated into sulfate, and O_2. This conversion is done by adopting our estimation of O_2^*-O_2 fractionation as $\Delta\delta^{18}O = -8.8$ ‰ (see discussion in section 3.1) and adopting the triple oxygen isotope exponent $C = 0.52$ in order to calculate $\Delta^{17}O_{O2}$. Our choice of this C value is admittedly arbitrary, representing

a generic mass-dependent triple oxygen isotope slope, whereas an arbitrary value of 0.5110 was similarly chosen for the kinetic isotope effect between sulfate and O_2 found in Cao and Bao (2021). The use of a 0.5110 slope, instead of 0.52, would shift the O_2^*-based $\Delta^{17}O_{O2}$ estimate lower by −0.08 ‰, and as such, we consider 0.52 as conservative.

2.4. METHODS: SULFATE TRIPLE OXYGEN ISOTOPE MEASUREMENTS AND DATA TREATMENT

For this study we measured the triple oxygen isotope composition of aliquots of the same purified barium sulfate ($BaSO_4$) sample extracts that were measured for $\delta^{34}S$, $\Delta^{33}S$, $\Delta^{36}S$, and $\delta^{18}O$ by Killingsworth et al. (2019), with details of the sample extraction in that prior study. Sulfate was extracted from powdered sedimentary rock samples from drill core 3 from the Turee Creek Drilling project (~2.3 Ga, see Philippot et al., 2018). The $\Delta^{17}O$ values of sulfate and a silicate reference standard were measured from evolved O_2 using a CO_2-laser fluorination (using BrF_5) technique (Bao and Thiemens, 2000) on a Thermo Finnigan Delta V Plus mass spectrometer in dual inlet mode using an in-house O_2 reference gas at the Institut de Physique du Globe de Paris (IPGP). The analytical uncertainty for the prior barite $\delta^{18}O$ measurements is ±0.4‰ (2σ) (Killingsworth et al., 2019), while barite measurements at IPGP are ±0.04‰ (2σ) for $\Delta^{17}O$ (Legendre et al., 2016), with both uncertainties based on replicate analysis of the NBS-127 $BaSO_4$ standard. Here, single samples of 3 to 6 mg of Kazput barite were measured for their $\Delta^{17}O$. During the same sample measurement sessions, replicates of the silicate standard UWG-2 (n=9) yielded an analytical uncertainty of ±0.04‰ (2σ) for $\Delta^{17}O$.

Non-quantitative sample yields during triple oxygen isotope measurements of sulfates add another challenge to the normalization of $\Delta^{17}O$ data. Data treatment is therefore required for normalization of $\Delta^{17}O$ against VSMOW (Miller et al., 2020) and to compensate for associated mass dependent fractionation (Cowie and Johnston, 2016). The analytical oxygen-isotope fractionation slope was determined from a linear regression of the $\delta'^{17}O$ versus $\delta'^{18}O$ of long-term measurements (n=66) of barite standard NBS-127, removing outliers beyond ±1σ of the mean. Using the determined slope, measured sample $\delta'^{17}O$ data were recalculated to the anchor point of the accurate $\delta'^{18}O$ versus VSMOW previously obtained via quantitative EA-coupled mass spectrometry (Killingsworth et al., 2019). This slope, C = 0.5158 (standard error ±0.0069), is likely the result of multiple fundamental processes. In contrast, a slope close to the high-temperature limit θ = 0.5305 may be determined from the CO_2-laser fluorination of barite using F_2 instead of BrF_5 (Cowie and Johnston, 2016). The target for NBS-127 of $\delta^{18}O_{VSMOW}$ = 9.3 ±0.3 ‰ (Gonfiantini et al., 1995) was used for ease of comparison against prior work that adopts similar values; however, more accurate interlaboratory comparisons have yielded NBS-127 $\delta^{18}O_{VSMOW}$ = 8.59 ±0.26 ‰ (Brand et al., 2009). Use of the latter value for our data correction would result in a slightly higher $\Delta^{17}O_{0.528}$ value, increasing our data by +0.009 ‰, well within the analytical uncertainty. Next, the barite sample $\delta'^{17}O$ value that has been treated for analytical fractionation is then normalized to VSMOW by applying the $\delta'^{17}O$ offset between the silicate standard UWG-2 from our raw (versus IPGP lab reference O_2) sample-session measurements and UWG-2 recently normalized against VSMOW-VSLAP (Miller et al., 2020). To do this, again, the $\delta'^{17}O$ data measured from UWG-2 are first corrected using the slope obtained from $\delta'^{17}O$-$\delta'^{18}O$ long-term data, ±1σ (n=337) of the $\Delta'^{17}O$ mean

of the raw data measured at IPGP, with the slope obtained being C = 0.5300 (standard error ±0.0038). As compared to the value of the triple oxygen slope obtained from the NBS-127 replicates, this slope for UWG-2 may have further meaning because it is close to the high temperature limit of 0.5305, and it is coming from the near-quantitative measurement of silicates (UWG-2) as compared to the partial yields of barites (NBS-127) during laser fluorination with BrF_5. Our UWG-2 data from the sample sessions (n=9), slope-corrected to the target of $\delta'^{18}O_{VSMOW}$ = 5.734 ‰ (Miller et al., 2020), give an offset of $\Delta\delta'^{17}O$ = +0.0259 ‰ between our data versus the $\delta'^{17}O$ = 2.982 ‰ of UWG-2 from Miller et al. Thus, the 2-step correction to put our barite oxygen-17 data on the VSMOW scale was done as follows:

$$\delta'^{17}O_{corr1} = \delta'^{17}O_{refgas} + 0.5158 \times (\delta'^{18}O_{VSMOW} - \delta'^{18}O_{refgas}) \quad (13),$$

where $\delta'^{1x}O_{refgas}$ is the raw data that is versus the IPGP laboratory working O_2 reference gas, and $\delta'^{18}O_{VSMOW}$ is the sample data previously obtained via EA (Killingsworth et al., 2019), followed by the correction to place the oxygen-17 data in the VSMOW reference frame,

$$\delta'^{17}O_{VSMOW} = \delta'^{17}O_{corr1} + 0.0259 \quad (14).$$

As a test of our correction, we applied (13) and (14) to the long-term IPGP NBS-127 data returning a mean of $\Delta'^{17}O_{0.528,VSMOW}$ = −0.03 ‰, comparing well with the $\Delta'^{17}O_{0.528,VSMOW}$ = −0.04 ‰ resulting from quantitative graphite reduction + CO_2 fluorination of NBS-127 (Bao and Thiemens, 2000). A comparison between the measured and corrected triple oxygen isotope data is shown in the supplementary information (Fig. S1).

3. RESULTS AND DISCUSSION

3.1. REASSESSING SULFATE-WATER $\delta^{18}O$ SIGNALS IN SULFATE

Our compilation of paired sulfate-water data from the oxidation of different sulfur species (Fig. 3) shows the $\delta^{18}O$ difference between sulfate and ambient water ($\Delta\delta^{18}O_{sulfate-water}$) varies from −77.3 ‰ (Krouse et al., 1991) to +34.7 ‰ (Sun et al., 2015). Such scatter is inconsistent with narrow ranges of H_2O- and O_2-oxygen in sulfate and constant sulfate-water fractionation factors. Most of the sulfate-water $\delta^{18}O$ data could be seen as a result of mixing between water-oxygen (with $\Delta\delta^{18}O_{sulfate-water} \approx 0$) and fractionated O_2-oxygen ($\Delta\delta^{18}O_{O2^*-O2} < 0$) end members, the latter of which we designate O_2^*. Measurements of the initial and residual O_2 involved in the oxidation of sulfides, such as pyrite, indicate a relatively limited range for $\Delta\delta^{18}O_{O2^*-O2}$ = −4.3 to −11.4 ‰ (Lloyd, 1968; Taylor et al., 1984; Oba and Poulson, 2009; Heidel and Tichomirowa, 2010), with an average of −8.8 ‰ that is adopted here. Dual isotope (i.e., $\delta^{18}O$) results are used for constraints in this case because $\Delta\Delta^{17}O_{O2^*-O2}$ during sulfide oxidation is yet to be experimentally determined. We suggest that the relatively limited range of $\Delta\delta^{18}O_{O2^*-O2}$ and the homogeneous isotope composition of atmospheric O_2 make O_2 a suitable anchor point to characterize the sulfate-water-O_2 oxygen isotope system, and to be used instead of $\Delta\delta^{18}O_{sulfate-water}$ that has been used for the same purpose (e.g., Van Stempvoort and Krouse, 1994; Balci et al., 2007; Calmels et al., 2007; Hemingway et al., 2020). We add the average $\Delta\delta^{18}O_{O2^*-O2}$ to atmospheric O_2 ($\delta^{18}O$ = 24.15 ‰; Pack et al., 2017) to estimate $\delta^{18}O_{O2^*}$ = 15.4‰. The evidence in Fig. 3 is consistent with our $\delta^{18}O_{O2^*}$, where $\Delta\delta^{18}O_{sulfate-water}$ is negative when $\delta^{18}O_{water} > \delta^{18}O_{O2^*}$ = 15.4 ‰, while $\Delta\delta^{18}O_{sulfate-water}$ is generally positive for $\delta^{18}O_{water} < \delta^{18}O_{O2^*}$ = 15.4 ‰. When viewed together here, the field and experimental data show a range of $\Delta\delta^{18}O_{sulfate-water} > 100$ ‰ and sulfate oxygen isotope compositions that match 100

% water-oxygen and 100 % O_2^*-oxygen. Most of the sulfates appear to contain <60 % O_2^*-oxygen, while there is no *a priori* reason to exclude even higher contributions from O_2 in some circumstances. For example, initially produced sulfates suggest incorporation of >75 % molecular oxygen in oxidation experiments with pyrites of grain sizes < 63 µm (Tichomirowa and Junghans, 2009; Heidel and Tichomirowa, 2010). At the very least, it is apparent that sulfates exceed the 8 to 15 % O_2-oxygen contribution (Balci et al., 2007) that was previously assumed in models (e.g., Bao et al., 2008; Crockford et al., 2019). Therefore, in our assessment here, such limits on sulfate's proportion of O_2-oxygen cannot be assumed in advance.

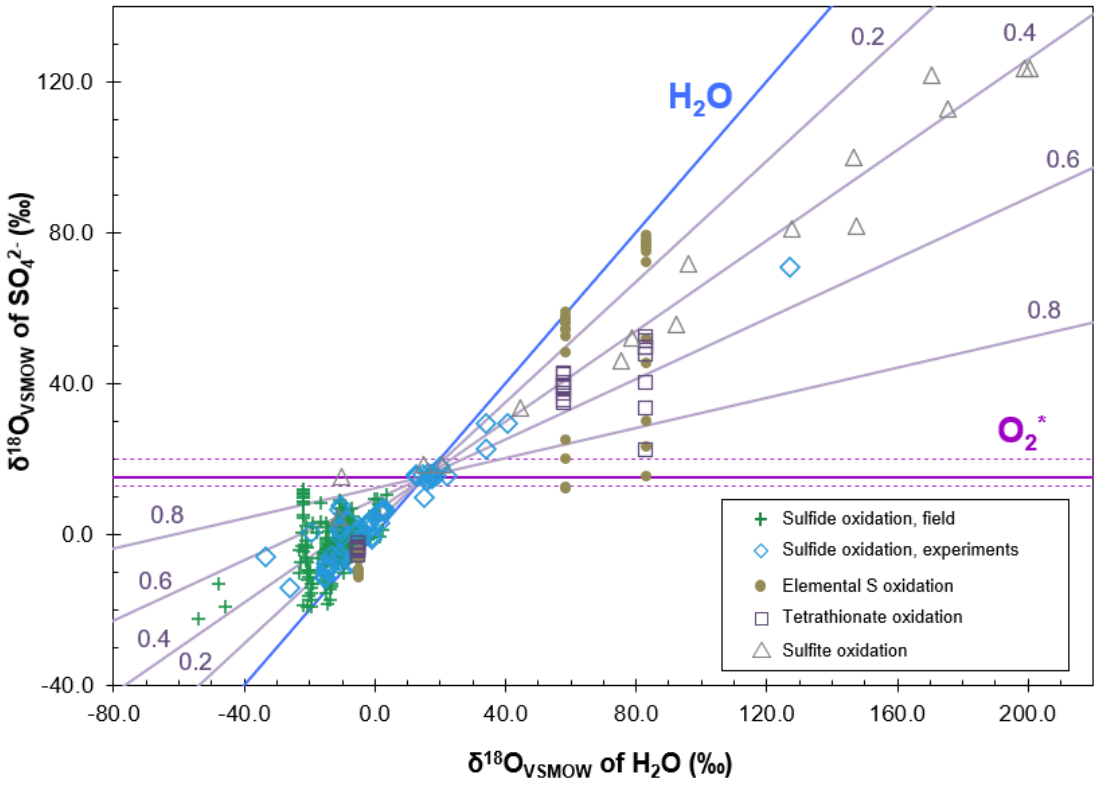

Figure 3. A compilation of experimental and field dissolved sulfate oxygen isotope data in cross-plot against paired ambient water oxygen isotope data. The data references are the same as in Figure 1. Here it is illustrated how sulfate-water oxygen-isotope fractionation

ranges both positive and negative, depending on the relationship between ambient water and fractionated O_2 during oxidation of reduced sulfur species to sulfate. Curves for sulfate end member cases, as described in the main text, are labeled and shown as H_2O = 100 % water-oxygen and O_2^* = 100 % fractionated O_2-oxygen. The numbered lines show the fractional incorporation of O_2^*-oxygen. Dashed lines for the horizontal O_2^* end member indicate its reported ranges, while the solid horizontal line is its average.

3.2. TESTING THE MODEL AGAINST EXTANT RECORDS OF PROTEROZOIC EXTREME OXYGEN-17 DEPLETIONS

Extreme negative $\Delta^{17}O_{sulfate}$ data are associated with the ~635 Ma Neoproterozoic Marinoan Snowball Earth meltdown and from earlier Proterozoic sulfates (Fig. 4). Such data are unambiguous in requiring an O_2-oxygen end member because atmospheric O_2 is the only suitable oxidant of sulfide that has a mass-independent ^{17}O-deficit. The upper bounds of the anomalous $\Delta^{17}O$-$\delta^{18}O$ data of Proterozoic sulfate generally conform to the Global Meteoric Water line, consistent with 100 % water-oxygen end members. Meanwhile, the minimum pCO_2 for the meltdown of a Snowball Earth event has been estimated to be 100 mbar of CO_2 (Hoffman et al., 2017). We use this pCO_2 in our model to determine not only an extreme ^{17}O-depletion for O_2 ($\Delta^{17}O_{O2} \leq -16.5$ ‰), but also strongly negative $\delta^{18}O_{O2}$ values (≤ -12 ‰), the latter of which has not been addressed previously. These approximations are conservative with respect to the $\Delta^{17}O$ record of sulfate and for pCO_2 because the other main control on the isotope composition of O_2, the photosynthetic O_2 flux, is set at modern levels for these estimates. Lowering pCO_2 and/or photosynthetic O_2 flux would further decrease $\Delta^{17}O_{sulfate}$ and $\delta^{18}O_{sulfate}$ values, as these values would respond to the isotope composition of O_2 as it tracked further downwards along the O_2 model curve in Fig. 4.

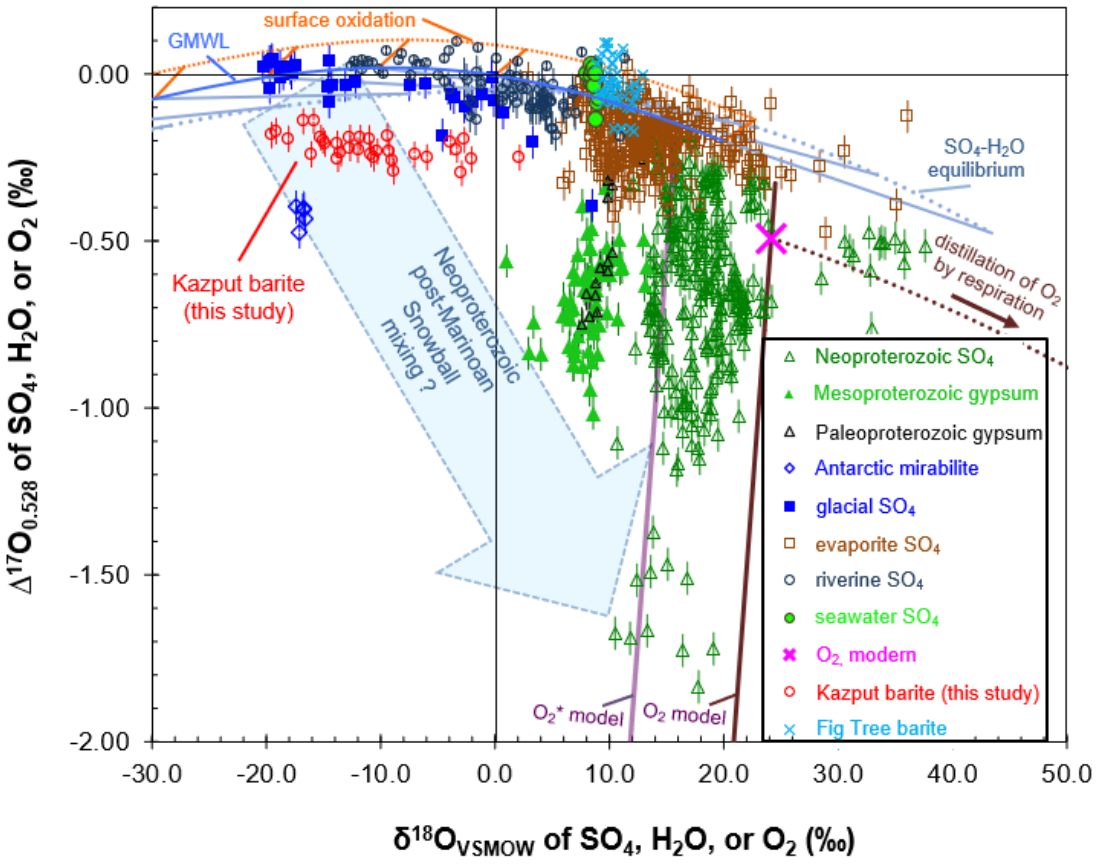

Figure 4. Kazput barite $\Delta^{17}O$ data and model O_2 results are shown from this study alongside published sulfate triple oxygen isotope data ($\Delta^{17}O$ and $\delta^{18}O$) from compiled and original sources (Crockford et al., 2019) with additional data (Sun et al., 2015; Kim et al., 2017; Killingsworth et al., 2019; Zhang et al., 2020; Peng et al., 2013; Waldeck et al., 2019; Hemingway et al., 2020). The sulfate data are presented together with the caution that they are not all corrected for mass-dependent fractionation during partial fluorination yields, and that they are not universally normalized to the same accepted values for reference standards. As such, discrepancies may exist on the order of ~0.1 ‰ for $\Delta^{17}O$. Error bars are shown for $\Delta^{17}O$ and are smaller than the symbols for $\delta^{18}O$. The Global Meteoric Water Line (GMWL) (Sengupta et al., 2020) represents the distillation (lighter $\delta^{18}O$) and evaporation (heavier $\delta^{18}O$) of meteoric waters as compared to their seawater source at the origin (represented by the isotope standard VSMOW at $\Delta^{17}O = \delta^{18}O = 0$ ‰). The composition of modern O_2 is also shown (Pack et al., 2017). Highly ^{17}O-anomalous sulfates, with isotopic arrays that extend in a more vertical orientation, are noted for the Paleoproterozoic, Mesoproterozoic, and Neoproterozoic. These anomalous arrays display the negative correlation between ^{17}O and ^{18}O that is predicted by the modeled curves for the variation in the triple oxygen isotope composition of O_2 as it tracks increasing pCO_2 and/or decreasing strength of biological O_2 fluxes. The model is also mirrored in the curve

for the fractionated O_2^* that is incorporated into sulfate. Fractionation curves for surface oxidation and sulfate in equilibrium with water (equilibrium) are calculated according to Cao and Bao (2021), with the curves shown as the labeled dotted lines with tie lines to meteoric water compositions. The possible trajectory of Rayleigh fractionation of atmospheric O_2 during distillation by respiration is labeled. A potential oxygen-isotope mixing trajectory for Neoproterozoic post-Marinoan Snowball sulfates is shown with the large shaded arrow.

If negative $\Delta^{17}O_{O2}$ and $\delta^{18}O_{O2}$ signals were incorporated into sulfate during continental sulfide oxidation in the glacial aftermath, then the sulfate triple oxygen isotope data should show mixing between high-low $\Delta^{17}O$-$\delta^{18}O$ of continental meteoric waters and low-high $\Delta^{17}O$-$\delta^{18}O$ atmospheric O_2. Such mixing would fall within the trajectory of the large shaded arrow in Fig. 4 like the few samples of Antarctic mirabilite near $\delta^{18}O = -20$ ‰ and $\Delta^{17}O = -0.5$ ‰ (Sun et al., 2015) that fall below the typical range of glacial sulfate, but this does not appear to be the case. Instead, the anomalous Neoproterozoic sulfates show a near-vertical $\Delta^{17}O$-$\delta^{18}O$ relationship within the lower right quadrant, indicative of mixing between evaporated water-oxygen (potentially seawater) and O_2-oxygen sources. Furthermore, the Neoproterozoic sulfate array contrasts sharply with the most $\delta^{18}O$-negative sulfates found in rocks, which are from Neoproterozoic diamictites (upper left-most data plotted on Fig. 4; Peng et al., 2013); whereas mixing between the Neoproterozoic glacial and anomalous (vertical array) sulfates is not apparent.

In a back-of-the-envelope calculation we estimate $\Delta^{17}O_{O2,0.528}$ using the average Marinoan sulfate ($\Delta^{17}O = -0.66$ ‰), the average O_2^*-oxygen ratio of sulfate (0.315) from our compilation (Fig. 4), and an evaporated water source ($\Delta^{17}O = -0.2$ ‰). The post-Marinoan Snowball O_2 is thus estimated at $\Delta^{17}O = -1.7$ ‰, close to the minimum sulfate data at $\Delta^{17}O = -1.84$ ‰ (Bao et al., 2009). This scenario suggests two important features. First, our

findings from paired sulfate and water $\delta^{18}O$ show that sulfate can contain as much as 100 % O_2^{*}-oxygen (Fig. 3), which implies that the Neoproterozoic $\Delta^{17}O$ minimum of sulfate may be notable not only for its extremity, but also for recording the composition of O_2 itself. Second, according to our model assessment, the Neoproterozoic sulfate $\Delta^{17}O$-$\delta^{18}O$ record may only require $pCO_2 \approx 3.2$ mbar, far short of the 100 mbar needed to deglaciate a Neoproterozoic Snowball Earth (Hoffman et al., 2017). As an aside, if we fix pCO_2 at 1 times present atmospheric levels (PAL), a fraction of 0.12 of present levels of pO_2 and photosynthetic O_2 flux (here, they are linked together, keeping O_2 residence time fixed at 1271 years) would be required for $\Delta^{17}O_{O2} = -1.7$ ‰. We reconcile these pCO_2 estimates, for now, by suggesting that the full $\Delta^{17}O$-$\delta^{18}O$ signal of O_2 responding to short-lived ultra-high CO_2 has not yet been observed in sulfates. If such extreme $\Delta^{17}O$ compositions of sulfate do exist, perhaps it will one day be feasible to observe this with *in situ* triple oxygen isotope measurements at the micro-scale.

Our model gives insight on earlier Proterozoic published $\Delta^{17}O$ data from sulfates as well. The Mesoproterozoic 1.4 Ga sulfates from the Sibley Group are interpreted as coming from a lacustrine setting (Crockford et al., 2018), displaying a loosely defined array (filled green triangles in Fig. 4) that is consistent with a stronger *strateff* on O_2 as compared to today and consistent with a lower-$\delta^{18}O$ water-oxygen source than the Marinoan case. The Mesoproterozoic Sibley Group sulfates occur below the evaporite field in Figure 4, reaching as low as $\Delta^{17}O_{sulfate,0.528} = -1.02$ ‰. The ^{17}O-anomalous 1.7 to 1.89 Ga Paleoproterozoic gypsum data (Crockford et al., 2019) show a very similar pattern to the Sibley Group sulfates, falling within the same $\Delta^{17}O$-$\delta^{18}O$ region (open black triangles in

Fig. 4), in sub-vertical arrays reaching as low as $\Delta^{17}O_{sulfate}$ = −0.75 ‰. Similar to the Neoproterozoic case, we identify potential end members. Starting with a less-evaporated water end member at $\Delta^{17}O$ = −0.1 ‰, we use the averages of the 1.4 Ga ($\Delta^{17}O \approx -0.67$ ‰) and 1.7 to 1.89 Ga ($\Delta^{17}O \approx -0.53$ ‰) sulfates to estimate their corresponding $\Delta^{17}O_{O2}$ values at −2 ‰ to −1.6 ‰. The respective intervals' $\Delta^{17}O_{O2}$ could correspond to a pCO_2 of 4 to 2.9 mbar, which is on the order of these time intervals' minimum estimated pCO_2 whose regulation of the climate, in turn, may have been boosted by methane (Catling and Zahnle, 2020). Indeed, work on Proterozoic analogs has suggested CH_4 may have had a significant control on early climate (Cadeau et al., 2020). A more prominent role for atmospheric methane eases the need to invoke high ranges for the pCO_2 estimated for the Proterozoic, likewise being amenable with our rough approximation that the extant triple oxygen isotope record of sulfate may not require pCO_2 higher than 4 mbar (≈ 10 PAL) since 1.89 Ga.

3.3. ANOTHER LOOK AT EVAPORITE O-ISOTOPE RECORDS

Records of evaporite gypsum and anhydrite S- and O-isotope signals are invaluable for insight on coupled ocean-atmosphere redox changes through the Proterozoic and Phanerozoic (Claypool et al., 1980; Crockford et al., 2019). The shaded field within Figure 5 indicates O-isotope compositions that we expect for sulfates incorporating oxygen from modern seawater ($\delta^{18}O$ = 0 and $\Delta^{17}O$ = 0) and modern O_2 (large pink X, at $\delta^{18}O$ = 24.15 ‰, $\Delta^{17}O$ = −0.49 ‰ (Pack et al., 2017)), with O_2^* being the O_2-oxygen end member of sulfate, and water-oxygen end members represented by sulfate-seawater equilibrium (Cao and Bao, 2021) via microbial sulfate reduction and partial reoxidation (light blue curves).

The upper range of sulfate-water equilibrium is very similar to the Global Meteoric Water Line. Given our findings that calculated fractionations for the sulfate system do not closely describe measured data (Fig. 1), we suggest the upper bounds of sulfate data may indeed match the GMWL itself instead of a sulfate-water equilibrium curve offset from the GMWL. That most evaporite data fall into the shaded field in Fig. 5 suggests that oxygen isotope compositions of seawater, and perhaps O_2, have been largely stable since the Proterozoic. Such agreement implies strong feedbacks that maintain stable isotope compositions of O_2 despite drastic differences in pO_2 and pCO_2 between the Proterozoic and the Phanerozoic. Crucially, such stability could occur if the flux of photosynthetic O_2 has been maintained within the same order of magnitude as modern fluxes (the flux of *bioO2* in the model).

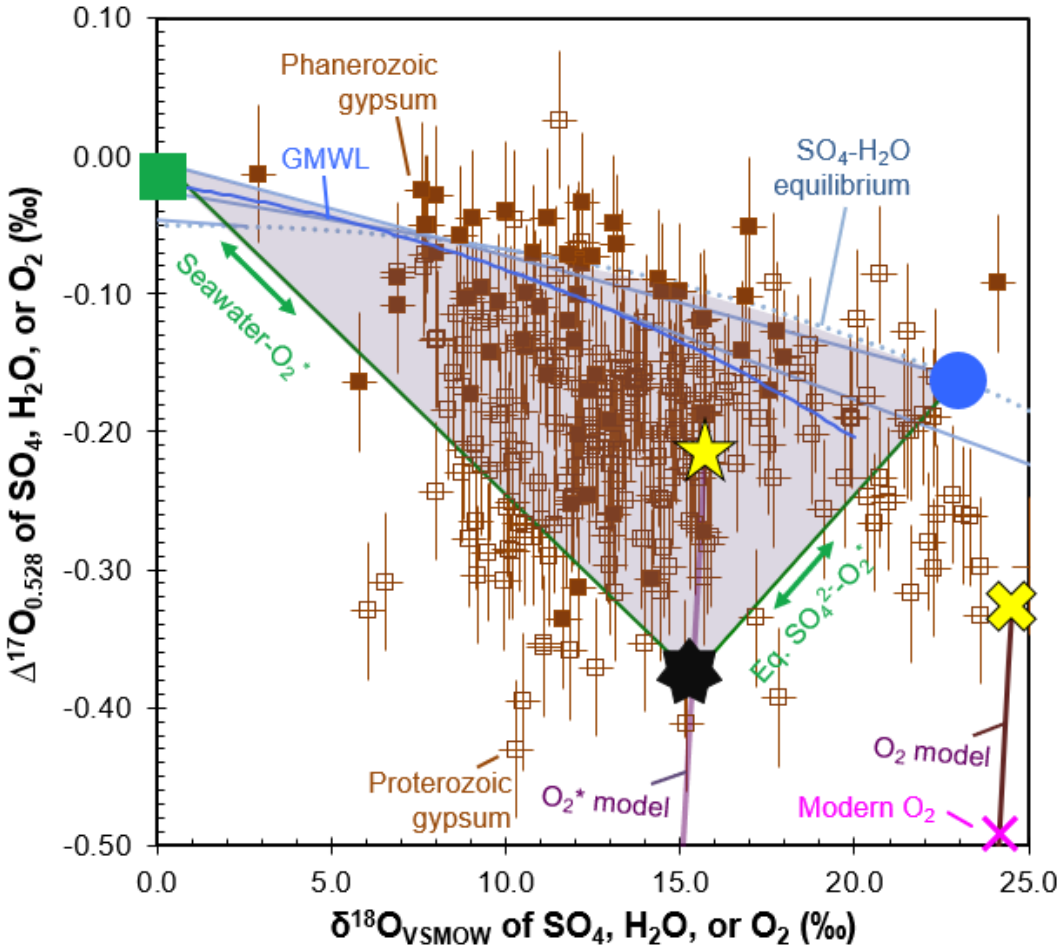

Figure 5. Compiled Phanerozoic and Proterozoic evaporite gypsum triple oxygen isotope data (Crockford et al., 2019) are shown here alongside the GMWL (Sengupta et al., 2020), sulfate-water equilibrium curve (Cao and Bao, 2021), and the composition of modern atmospheric O_2 (Pack et al., 2017). The shaded region is where sulfates formed from initial oxidation of sulfides in seawater or re-oxidation after microbial sulfate reduction may occur. Such sulfate would have oxygen sources from seawater (filled green square) and O_2^* (black multi-pointed star) with variable effects from the fractionation of residual sulfate caused by microbial sulfate reduction that pushes sulfate composition towards sulfate-seawater equilibrium (filled blue circle symbol). Biologically produced O_2 (yellow x symbol) and its respective O_2^* (yellow star) are discussed in the text.

Another aspect to be explored in the record of evaporites (and sulfates, generally) is possible incorporation of O_2-oxygen that is only from biologically produced O_2 (*bioO2* in the model) with no mixing of stratospheric O_2 (*strateff* in the model). Such O_2 would be

produced and consumed *in situ*, thus retaining no mass-independent signal while only registering the isotopic effects of photosynthetic O_2 production and biological respiration (see also Fig. 2). This O_2, and its corresponding O_2^*, are shown as the yellow X and star symbols, respectively, in Figure 5. We hypothesize that such oxygen signals might be possible under atmospheric pO_2 low enough for photosynthetic O_2 to be consumed *in situ* or diffuse into the atmosphere without diffusion of O_2 back into water from the atmosphere. Some Proterozoic evaporites are consistent with this possibility, spanning between *bioO2* and its corresponding O_2^*, while very few evaporite data plot in the area below the *bioO2*-*bio*O_2^* boundary and between the model curves for O_2^* and O_2. Meanwhile, the potential distillation of atmospheric O_2, which would follow a Rayleigh fractionation curve characterized by increasing $\delta^{18}O$ (Fig. 4), is not clearly observed in the triple oxygen isotope record of sulfate. We therefore suggest that atmospheric O_2 drawdown could be indicated in $\Delta^{17}O$-$\delta^{18}O$ space by sulfates that span across O_2^* and O_2 instead of tracking a Rayleigh distillation curve, possible, for example, in the case of the anomalous Neoproterozoic sulfates (Fig. 4).

3.4. IMPLICATIONS FOR THE EARLY PALEOPROTEROZOIC FROM KAZPUT BARITE $\Delta^{17}O$

The study section of the W. Australia lower Kazput Formation of the Turee Creek Group consists of an interval, ~60 meters thick, of drill core of finely laminated mud- and siltstones bracketing a carbonate-rich interval (Killingsworth et al., 2019). Absolute age constraints place the Kazput Formation between 2.31 to 2.2 Ga (Philippot et al., 2018; Caquineau et al., 2018), while detailed sedimentary context is available elsewhere (e.g.,

Van Kranendonk et al., 2015; Barlow et al., 2016). Prior quadruple sulfur and oxygen-18 isotope results from the Kazput barite, which features unusually low $\delta^{18}O$, were interpreted in favor of sulfate derived from continental sulfide oxidation being precipitated as barium sulfate (barite) within a possibly restricted basin between 2.31 to 2.2 billion years ago (Killingsworth et al., 2019). Trace element and *in situ* microanalysis of sulfur isotopes (Philippot et al., 2018) and additional petrologic evidence (Killingsworth et al., 2019) have ruled out post-depositional oxidation of pyrite as the source of sulfate for Kazput barites.

Our $\Delta^{17}O$ data (n = 32) of Kazput barite range from −0.30 ‰ to −0.14 ‰ with a mean of −0.22 ‰ (Table 4). A regression of the $\Delta^{17}O$ of Kazput barite with its prior $\delta^{18}O$ data intersects the Global Meteoric Water Line at $\delta^{18}O$ = −35.5 +3.5/−5 ‰ (2σ) and $\Delta^{17}O$ = −0.13 +0.03/−0.05 ‰ (2σ) (Fig. 6). These values constrain the sulfate's water end member, which previously was not possible with the $\delta^{18}O_{sulfate}$ data alone. This water-oxygen source is within range of the Paleoproterozoic Snowball Earth meltwater source estimated at $\delta^{18}O$ = −43 ±3 ‰ (1σ) that was invoked for hydrothermal alteration of ca. 2.3-2.4 Ga silicate rocks (Herwartz et al., 2015). Although it is uncertain if these Paleoproterozoic records of ^{18}O-depleted waters are from the same time period or not, at the least they both indicate sources of glacial meltwaters from within the ca. 2.4-2.2 Ga interval of extensive global glaciations (Gumsley et al., 2017). In the case of the Kazput barite, such a record of meltwater is consistent with recent suggestions of an additional younger glacial unit within the Turee Creek Group succession (Martin, 2020; Philippot et al., 2021).

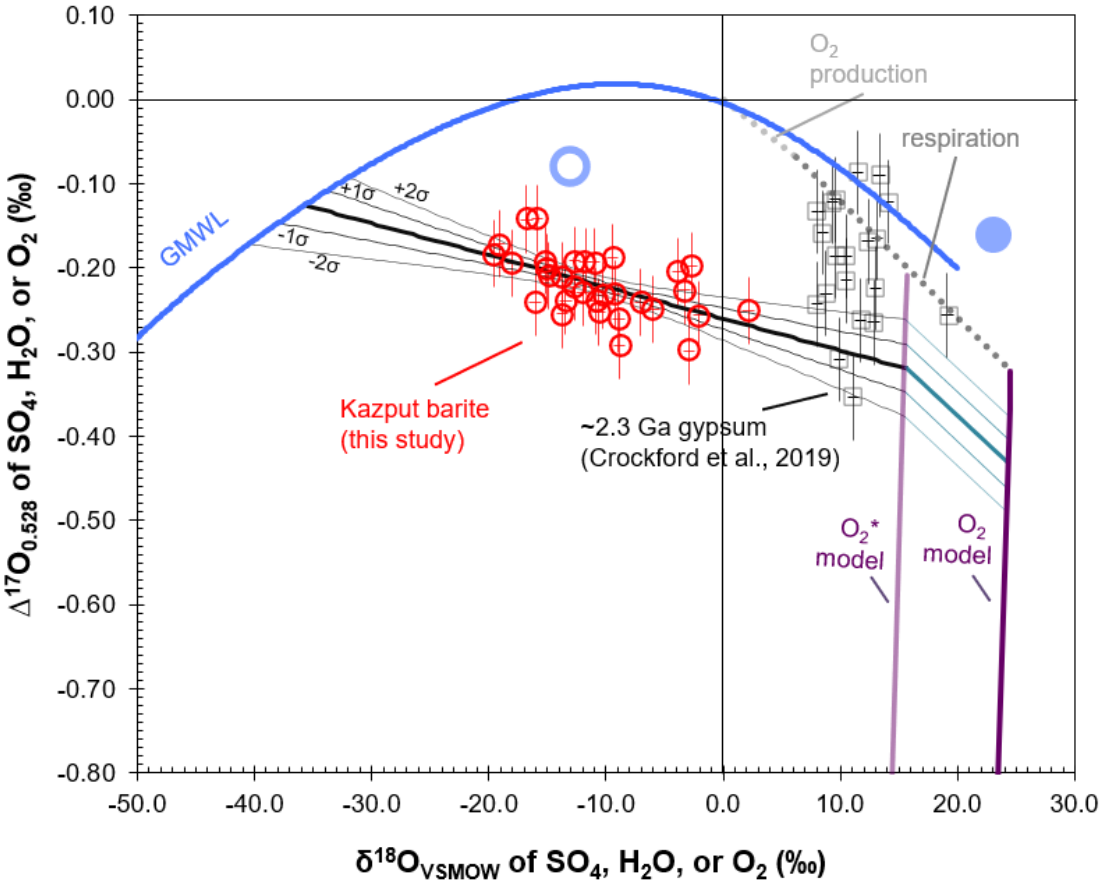

Figure 6. Results of Kazput barite triple oxygen isotope measurements (open circles) from this study are shown in $\Delta^{17}O$-$\delta^{18}O$ space. The Global Meteoric Water Line (GMWL) is a curve fit after Sengupta et al. (2020). In the O_2 system, the constraints used for biological O_2 production and respiration in our model are shown by the respective labeled curves, while the modeling of the stratospheric effect on O_2 that is attributed to pCO_2 concentrations is shown as the O_2 model. The O_2^* model denotes our estimation of the fractionated O_2 that is incorporated into sulfate, which is tied to the O_2 model. A linear regression of the mixing between Kazput barite oxygen isotope end members is shown along with ±1σ and ±2σ of the mean, with the intersection of the regression with the GMWL and the O_2 model curves allowing estimation of the respective water- and O_2-oxygen end members for the Kazput sulfate oxygen sources. The compositions of sulfate-water equilibrium with respect to the Kazput sulfate water end member and seawater are shown as the large open and filled circle symbols, respectively. Evaporite (gypsum) data from 2.3 Ga from Crockford et al. (2019) are shown for comparison.

Table 4
Triple oxygen isotope measurements of Kazput barite. The $\delta^{18}O$ data are from Killingsworth et al. (2019), $\Delta^{17}O$ data are from this study.

Sample name	$\delta^{18}O_{VSMOW}$ (‰) (Killingsworth et al., 2019)	$\Delta^{17}O_{VSMOW,0.528}$ (‰) (this study)
CAS 1	-6.0	-0.25
CAS 3	-15.0	-0.20
CAS 4	-2.7	-0.20
CAS 5	-9.4	-0.19
CAS 6	-12.7	-0.22
CAS 8	-12.7	-0.19
CAS 9	-16.8	-0.14
CAS 10	-13.8	-0.21
CAS 11	-16.1	-0.24
CAS 13	-18.0	-0.19
CAS 14	-11.8	-0.19
CAS 15	-15.2	-0.19
CAS 16	-9.2	-0.23
CAS 18	-8.9	-0.26
CAS 19	-19.5	-0.18
CAS 20	-3.9	-0.20
CAS 21	-12.0	-0.23
CAS 23	2.2	-0.25
CAS 24	-14.9	-0.21
CAS 26	-10.8	-0.24
CAS 28	-19.1	-0.17
CAS 29	-13.5	-0.24
CAS 30	-15.9	-0.14
CAS 31	-11.0	-0.19
CAS 33	-10.6	-0.25

CAS 34	-10.3	-0.23
CAS 35	-2.9	-0.30
CAS 36	-7.0	-0.24
CAS 38	-8.8	-0.29
CAS 39	-13.7	-0.25
CAS 40	-3.3	-0.23
CAS 41	-2.1	-0.26
Analytical uncertainty based on replicates of the NBS-127 $BaSO_4$ standard	±0.4‰ (2σ)	±0.04‰ (2σ)

Compared to its meltwater source, the Kazput sulfate isotopic array also requires a more ^{17}O-depleted and ^{18}O-enriched oxygen isotope end member. Existing sulfates from ~2.3 Ga could represent an ^{18}O-enriched end member for the Kazput barite, but their occurrence, as evaporite gypsum, and their mass-dependent $\Delta^{33}S$ data being less than 0.07 ‰ (Crockford et al., 2019) are both inconsistent with the Kazput sulfate meltwater oxygen source and its $\Delta^{33}S$ range between 0.6 ‰ to 1.6 ‰ (Killingsworth et al., 2019). An influence from microbial sulfate reduction (MSR) would push residual sulfate closer to sulfate-water oxygen isotope equilibrium with either the Kazput water end member or seawater, but this is not observed in the Kazput barite data array (Fig. 5). Neither was the influence of MSR on Kazput barite sulfur-oxygen isotope correlations observed previously (Killingsworth et al., 2019). Meanwhile, the minimum $\Delta^{17}O$ of −0.35 ‰ previously observed in the ~2.3 Ga gypsum (Crockford et al., 2019) is consistent with the atmospheric O_2 implied by the Kazput barite, attesting to their approximately time-equivalent global O_2 source. Our estimate of the Kazput sulfate O_2^* end member, by regression of the sulfate

data array to its intersection with our modeled O_2 curves, translates to an O_2 with $\Delta^{17}O$ = −0.43 +0.05/−0.06 ‰ (2σ) and $\delta^{18}O$ = 24.3 ±0.1 ‰ (2σ) (Fig. 6).

The $\Delta^{33}S$ signals from Kazput barite that are larger than +0.3‰ (Killingsworth et al., 2019) imply an anoxic atmosphere (O_2 <10^{-5} PAL; Pavlov and Kasting, 2002), while in an apparent paradox, the oxygen end member for Kazput barite with $\Delta^{17}O$ < −0.32 ‰ (lower than biologically produced O_2, as determined in this study) suggests a stable ozone layer with O_2 >10^{-2} PAL (Gregory et al., 2021). An older point of reference is found in Archean, ca. 3.2 Ga, Fig Tree barite, but these differ from the Kazput case in having negative $\Delta^{33}S$ signals (average = −0.55 ‰) and $\Delta^{17}O$-$\delta^{18}O$ data scattering near modern seawater sulfate and the GMWL (Fig. 4; Bao et al., 2007). For the waning $\Delta^{33}S$ signals of anoxia that occur after 2.45 Ga, Farquhar and Wing (2003) first gave two hypotheses: 1) sulfide-derived sulfate may retain the sulfur isotope signatures of their weathering sources even though the atmosphere was sufficiently oxygenated to shut down contemporaneous generation and preservation of $\Delta^{33}S$ > ±0.3 ‰, or 2) after 2.45 Ga the atmosphere was oscillating between anoxic and oxic states (above and below the 10^{-5} PAL threshold) that allowed episodic generation and preservation of primary atmospheric sulfur with $\Delta^{33}S$ > ±0.3 ‰. The first hypothesis was expanded further to show such low-T sedimentary recycling of sulfur anomalies could prolong their specifically positive-sign ($+\Delta^{33}S$) signals under an oxygenated atmosphere to a maximum $\Delta^{33}S$ around +2 ‰, with this memory effect disappearing below +0.3 ‰ by ~200-250 Myrs (Reinhard et al., 2013; Philippot et al., 2018). The second hypothesis has recently been supported by the interpretation of the reappearance $\Delta^{33}S$ signals of pyrite reaching up to +2.7 ‰, indicating a return of

atmospheric anoxia before ~2.2 Ga (Poulton et al., 2021). Meanwhile, two persistent features stand out in this 2.45 Ga to 2.2 Ga interval of the Great Oxidation and beyond: 1) since 2.42 Ga, there are only positive, and no negative, $\Delta^{33}S$ anomalies preserved in rocks (Killingsworth et al., 2019), and 2) since 2.4 Ga, $\Delta^{17}O$ of sulfate indicates a stable ozone layer (Crockford et al., 2019). Therefore, we suggest that the indication of positive $\Delta^{33}S$ and negative $\Delta^{17}O$ anomalies from Kazput barite at ~2.3 Ga are most readily explained by sedimentary recycling of $\Delta^{33}S$ anomalies under an oxygenated atmosphere of at least 10^{-2} PAL O_2, which is consistent with the evidence for irreversible oxygenation by ca. 2.4 Ga (e.g., Crockford et al., 2019; Warke et al., 2020), and waning signals of recycled sulfur anomalies until a maximum of ca. 2.2 Ga (Reinhard et al., 2013; Philippot et al., 2018).

As pO_2, pCO_2, and GPP are all effective 'levers' on $\Delta^{17}O_{O2}$ variation, additional constraints are needed to return unique inverse model solutions from a given $\Delta^{17}O_{O2}$ value. As has been done before, for example by Crockford et al. (2019), we assume that the flux of *bioO2* is proportional to GPP. The model is then inverted to solve for GPP from a given O-isotope composition by applying our sulfate isotope constraints on O_2 from Kazput barite, then resampling the model with a Monte Carlo treatment to constrain ranges of GPP. The Kazput barite-constrained $\Delta^{17}O_{O2}$ used in the model is −0.43 +0.03 ‰ (1σ) (Fig. 6). We use the same starting point as Crockford et al. (2019) for the early Paleoproterozoic, based on estimates of atmospheric gas concentrations of pO_2 = 0.001 to 2 (10^{-4} to $10^{0.3}$) and pCO_2 = 10 to 80 at ~2.3 Ga, both with respect to their present atmospheric levels (PAL). We further test this pO_2 range in our model to down below the threshold of the disappearance of sulfur isotope mass-independent fractionation, 10^{-5} PAL, going all the way down to 0

PAL. The relative importance of land versus marine O_2 production in the early Earth is unclear as evidence implies life was already on land in the Archean (e.g., Thomazo et al., 2018; Homann et al., 2018). Thus, we do not change relative contributions, running our model with total land and marine O_2 production inclusive as a ratio of present *bioO2* flux, which is proportionally equivalent to GPP versus present levels. Furthermore, we estimate the isotopic difference between terrestrial and marine contributions to O_2 to be small, within $\Delta\delta^{18}O \leq 0.3$ ‰, a difference that can be neglected in the model considering the much greater uncertainties surrounding pCO_2, pO_2, and total O_2 flux. We do not assume limits on the specific proportion of O_2 signal that can be registered in sulfate, though this is the approach used in previous works (e.g., Cao and Bao, 2013; Planavsky et al., 2020). In contrast, our triple oxygen isotope approach may attribute a less-negative $\Delta^{17}O_{O2}$ value from sulfate constraints. For our approach to be most effective, sulfate records with meteoric, instead of oceanic, water end members are needed. The effectiveness can be seen in Figure 5, where the $\Delta^{17}O$-$\delta^{18}O$ array of the Kazput barite is compared to published evaporite sulfate records from around the same time (~2.3 Ga; Crockford et al., 2019). The low $\delta^{18}O$ value of its water end member makes the $\Delta^{17}O$-$\delta^{18}O$ array of the Kazput barite intersect its O_2 end member at a lower angle as compared to the near-vertical approach of the evaporite data. In effect, these sulfate data from ~2.3 Ga are consistent with one another, though their interpretation differs with the minimum $\Delta^{17}O$ data of evaporites previously assumed to contain a maximum of 15 % O_2-oxygen (Crockford et al., 2019). Here we observe that, instead, the same evaporite with minimum $\Delta^{17}O$ might contain much closer to a maximum 100 % O_2-oxygen, or, more accurately, nearly 100 % O_2^*-oxygen. In another departure from prior approaches, we do not assume that the biosphere imparts O_2

with a $\Delta^{17}O$ value of 0, because, in fact, the biological production and respiration of O_2 do impart a significant mass-dependent triple oxygen isotope fractionation to O_2 on the order of $\Delta^{17}O \approx -0.3$ ‰ to -0.4 ‰ (Luz et al., 2014; Young et al., 2014; Fig. 2), that we calculate as $\Delta^{17}O = -0.32$ ‰ (see discussion on the *bioO2mod* in section 2.3). In sum, compared to prior approaches, here the net result is that we determine a less-negative $\Delta^{17}O_{O2}$ value from $\Delta^{17}O$ records of sulfate but a higher biological O_2 flux (i.e., GPP) because we account for the negative signal of $\Delta^{17}O_{bioO2}$.

Our model results with triple oxygen isotope constraints from Kazput barite suggest gross primary production was between 6 to 160 times (or $10^{0.8}$ to $10^{2.2}$) present levels at ~2.3 Ga with large fluxes of photosynthetic O_2 being required to balance 10^{-2} to $10^{-0.4}$ PAL pO_2 and pCO_2 of 10 to 80 times PAL (Fig. 7). These GPP results are higher than those found previously for ~2.3 Ga, which were 27.3 times present levels at maximum (Crockford et al., 2019). The GPP results that are below 10^{-2} PAL pO_2 fall outside of the 99.5 percentile, an independent confirmation that an oxygenated atmosphere may be unstable below this pO_2 horizon (Gregory et al., 2021). At higher pO_2, GPP becomes more sensitive to the range of pCO_2. Maximum pO_2 is limited here to 40 % ($10^{-0.4}$) PAL after constraints from Proterozoic ocean anoxia (Kump, 2008). Analysis of the burial of organic carbon through time indicates ~2.3 Ga may have had a comparably productive biosphere as the present (Krissansen-Totton et al., 2015), an implication that is in contrast to the demands from high pCO_2 of 10 to 80 PAL and potentially elevated GPP in the early Paleoproterozoic (Crockford et al., 2019). Enhanced efficiency of total carbon burial has also been invoked to balance such higher carbon inputs in the past (Kipp et al., 2021). However, recent

reinterpretation of the Paleoproterozoic Lomagundi-Jatuli carbon isotope excursion, which has previously been interpreted as a global-scale episode of enhanced carbon burial, suggests that surficial influxes and outfluxes of carbon have been in balance throughout Earth history (Prave et al., 2021). Meanwhile, our estimate of GPP between 6 to 160 present levels at ~2.3 Ga offers further support that the constraints imposed by records of carbon burial, indicators of high pCO_2, and sulfate triple oxygen isotopes may all be satisfied by a highly productive early Paleoproterozoic biosphere.

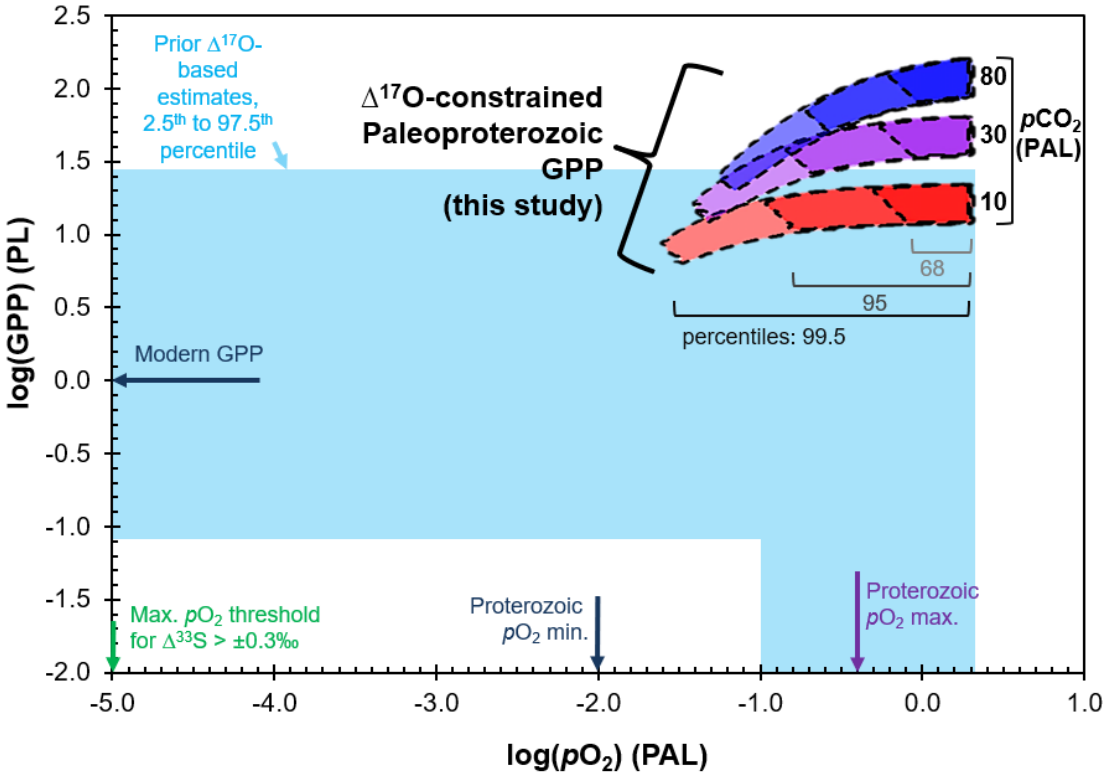

Figure 7. $\Delta^{17}O$-constrained model results of Paleoproterozoic gross primary production (GPP) from this study are shown in comparison with prior results from Crockford et al. (2019), all for ~2.3 Ga and shown as a function of pO_2 (x-axis) and different pCO_2 estimates (labeled curved fields). The Proterozoic pO_2 minimum is from Gregory et al. (2021), while the Proterozoic pO_2 maximum is taken from Kump (2008). Monte Carlo treatment of our inverted model constrains GPP results to within the percentiles labeled in the figure.

The simplifications being made here, and in prior studies, leave room for further exploration of controls on O_2 sources and sinks. For example, equating GPP with biological O_2 flux does not account for other O_2 fluxes such as permitted by pyrite formation. Ferrous iron or sulfide sinks of O_2 are not examined here either, whose inclusion in triple oxygen isotope-constrained GPP estimates would require an even higher GPP. Accounting for such other O_2 sources and sinks requires additional model constraints (e.g., Planavsky et al., 2020). From an oxygen-isotope perspective, however, we can use the full version of our *tropO2* model to further examine the effect of the biosphere on O_2 and its implications for GPP. For example, the need for more constraint on the oxygen isotope composition of photosynthetic O_2 is highlighted by the uncertainties surrounding global average leaf water (West et al., 2008; Young et al., 2014). Here we focus on respiration because this process is the most important isotopic control on biologically affected O_2. A lower efficiency of respiration for the Paleoproterozoic may have served as an additional source of O_2 by way of permitting more organic carbon burial. We test the implication of lowered respiration efficiency on triple oxygen isotope-constrained GPP to see if it would still require high GPP for the Paleoproterozoic, ca. 2.3 Ga. This is done with the caveat that the triple oxygen isotope slope of global respiration is still being refined (e.g., Ash et al., 2020). Decreasing efficiency of respiration will cause the upper bound of O_2 (biological O_2 without the stratospheric effect) to track along the triple oxygen isotope respiration slope towards photosynthetic O_2 production (Fig. 5). With the model set for maximum pO_2 at $10^{0.3}$ (2 PAL) and minimum pCO_2 at 10 PAL for ~2.3 Ga we can observe the minimum GPP required by the isotope composition of O_2 that is constrained by Kazput barite using the lower 1σ of the data regression curve (see also Fig. S3). Under those conditions, if

respiration were 2/3 of modern the minimum GPP would be 4.2 times present levels. Though unrealistic, we test the sensitivity to respiration efficiency by dropping respiration to zero, making the starting biological O_2 purely photosynthetic, before it is affected by mixing with stratospheric O_2. With no respiration, our constraints require a minimum GPP of 2.8 times present levels. Surprisingly, both cases affirm the requirement of higher GPP than modern for the early Paleoproterozoic, with slightly lower GPP than the minimum of 6 times present levels estimated in our prior simplified model runs.

4. CONCLUSION

Here, we provide a new framework in which to evaluate triple oxygen isotope records of sulfate. We show that triple oxygen isotope compositions of sulfate should be evaluated without pre-assigning the O_2/H_2O oxygen source ratio of sulfate, and that sulfate may contain a range of oxygen sources spanning 100 % H_2O-oxygen to 100 % O_2^*-oxygen (fractionated O_2-oxygen). Given additional constraints, distinguishing between the stratosphere and biosphere effects on $\Delta^{17}O_{O2}$ and $\delta^{18}O_{O2}$, and an accounting of the ancient Dole Effect via sulfate records, may now be more fully realized in the framework provided here. As an example, using sulfate $\Delta^{17}O$ and $\delta^{18}O$ constraints, we estimate early Paleoproterozoic gross primary productivity to be 6 to 160 modern levels, with a bare minimum threshold of 3 times modern levels. Such estimates of high productivity may reflect life's efficient expansion in an oxygenated world or that significant sources of O_2 remain to be accounted for.

FUNDING

This research was supported in part by funding from Fundação Amparo à Pesquisa do Estado de São Paulo (FAPESP grant 2015/16235-2 to P.P.) and the European Union's Horizon 2020 research and innovation program (Marie Sklodowska-Curie grant 708117 to B.K.).

ACKNOWLEDGEMENTS

The authors appreciate the constructive critiques by two anonymous reviewers and the editorial handling by Michael Böttcher. B.K. is grateful for the support of the USGS Mineral Resources Program. Any use of trade, firm, or product names is for descriptive purposes only and does not imply endorsement by the U.S. Government.

REFERENCES

Andrews, A.E., Boering, K.A., Daube, B.C., Wofsy, S.C., Loewenstein, M., Jost, H., Podolske, J.R., Webster, C.R., Herman, R.L., Scott, D.C., Flesch, G.J., Moyer, E.J., Elkins, J.W., Dutton, G.S., Hurst, D.F., Moore, F.L., Ray, E.A., Romashkin, P.A., Strahan, S.E., 2001. Mean ages of stratospheric air derived from in situ observations of CO 2, CH 4, and N 2O. Journal of Geophysical Research: Atmospheres 106 (D23), 32295–32314. doi:10.1029/2001JD000465.

Ash, J.L., Hu, H., and Yeung, L.Y., 2020, What Fractionates Oxygen Isotopes during Respiration? Insights from Multiple Isotopologue Measurements and Theory: ACS Earth and Space Chemistry, v. 4, p. 50-66, doi:10.1021/acsearthspacechem.9b00230

Balci, N., Brunner, B., and Turchyn, A.V., 2017, Tetrathionate and elemental sulfur shape the isotope composition of sulfate in acid mine drainage: Frontiers in Microbiology, v. 8, p. 1564.

Balci, N., Shanks, W.C., Mayer, B., and Mandernack, K.W., 2007, Oxygen and sulfur isotope systematics of sulfate produced by bacterial and abiotic oxidation of pyrite: Geochimica et Cosmochimica Acta, v. 71, p. 3796−3811, doi:10.1016/j.gca.2007.04.017.

Bao, H., 2015, Sulfate: A time capsule for Earth's O2, O3, and H2O: Chemical Geology, v. 395, p. 108−118, doi:10.1016/j.chemgeo.2014.11.025.

Bao, H., Cao, X. and Hayles, J.A., 2016, Triple oxygen isotopes: fundamental relationships and applications: Annual Review of Earth and Planetary Sciences, v. 44, p. 463-492, doi: 10.1146/annurev-earth-060115-012340.

Bao, H.M., Fairchild, I.J., Wynn, P.M., and Spotl, C., 2009, Stretching the Envelope of Past Surface Environments: Neoproterozoic Glacial Lakes from Svalbard: Science, v. 323, p. 119−122, doi:10.1126/science.1165373.

Bao, H., Lyons, J.R., and Zhou, C., 2008, Triple oxygen isotope evidence for elevated CO2 levels after a Neoproterozoic glaciation: Nature, v. 453, p. 504−6, doi:10.1038/nature06959.

Bao, H., Rumble, D., and Lowe, D.R., 2007, The five stable isotope compositions of Fig Tree barites: Implications on sulfur cycle in ca. 3.2 Ga oceans: Geochimica et Cosmochimica Acta, v. 71, p. 4868-4879, doi:10.1016/j.gca.2007.05.032.

Bao, H., and Thiemens, M.H., 2000, Generation of O2 from BaSO4 using a CO2-laser fluorination system for simultaneous analysis of δ18O and δ17O: Analytical chemistry, v. 72, p. 4029−4032.

Barlow, E., Van Kranendonk, M., Yamaguchi, K., Ikehara, M., and Lepland, A., 2016, Lithostratigraphic analysis of a new stromatolite−thrombolite reef from across the rise of atmospheric oxygen in the Paleoproterozoic Turee Creek Group, Western Australia: Geobiology, v. 14, p. 317−343.

Bender, M., Sowers, T., and Labeyrie, L., 1994, The Dole effect and its variations during the last 130,000 years as measured in the Vostok ice core: Global Biogeochemical Cycles, v. 8, p. 363−376.

Berner, R.A., 2006, GEOCARBSULF: A combined model for Phanerozoic atmospheric O2 and CO2: Geochimica et Cosmochimica Acta, v. 70, p. 5653−5664, doi:10.1016/j.gca.2005.11.032.

Blunier, T., Barnett, B., Bender, M.L., and Hendricks, M.B., 2002, Biological oxygen productivity during the last 60,000 years from triple oxygen isotope measurements: Global Biogeochemical Cycles, v. 16, p. 3-1-3−13, doi:10.1029/2001GB001460.

Brand, W.A. et al., 2009, Comprehensive inter-laboratory calibration of reference materials for δ18O versus VSMOW using various on-line high-temperature conversion techniques: Rapid Communications in Mass Spectrometry, v. 23, p. 999−1019, doi:10.1002/rcm.3958.

Cadeau, P. et al., 2020, Carbon isotope evidence for large methane emissions to the Proterozoic atmosphere: Scientific Reports, v. 10, p. 18186, doi:10.1038/s41598-020-75100-x.

Calmels, D., Gaillardet, J., Brenot, A., and France-Lanord, C., 2007, Sustained sulfide oxidation by physical erosion processes in the Mackenzie River basin: Climatic perspectives: Geology, v. 35, p. 1003-1006, doi:10.1130/G24132A.1.

Cao, X., and Bao, H., 2013, Dynamic model constraints on oxygen-17 depletion in atmospheric O2 after a snowball Earth: Proc Natl Acad Sci U S A, v. 110, p. 14546−50, doi:10.1073/pnas.1302972110.

Cao, X., and Bao, H., 2021, Small Triple Oxygen Isotope Variations in Sulfate: Mechanisms and Applications: Reviews in Mineralogy and Geochemistry, v. 86, p. 463−488, doi:10.2138/rmg.2021.86.14.

Caquineau, T., Paquette, J.-L., and Philippot, P., 2018, U-Pb detrital zircon geochronology of the Turee Creek Group, Hamersley Basin, Western Australia: timing and correlation of the Paleoproterozoic glaciations: Precambrian Research, doi:10.1016/j.precamres.2018.01.003.

Catling, D.C., and Zahnle, K.J., 2020, The Archean atmosphere: Science Advances, v. 6, p. eaax1420. doi: 10.1126/sciadv.aax1420

Claypool, G.E., Holser, W.T., Kaplan, I.R., Sakai, H., and Zak, I., 1980, The age curves of sulfur and oxygen isotopes in marine sulfate and their mutual interpretation: Chemical Geology, v. 28, p. 199−260.

Coplen, T., 2011, Guidelines and recommended terms for expression of stable-isotope-ratio and gas-ratio measurement results: Rapid Communications in Mass Spectrometry, v. 25, p. 2538−2560, doi:10.1002/rcm.5129.

Cowie, B.R., and Johnston, D.T., 2016, High-precision measurement and standard calibration of triple oxygen isotopic compositions (δ18O, Δ′17O) of sulfate by F2 laser fluorination: Chemical Geology, doi:10.1016/j.chemgeo.2016.07.003.

Crockford, P.W. et al., 2019, Claypool continued: Extending the isotopic record of sedimentary sulfate: Chemical Geology, doi:10.1016/j.chemgeo.2019.02.030.

Crockford, P.W., Hayles, J.A., Bao, H., Planavsky, N.J., Bekker, A., Fralick, P.W., Halverson, G.P., Bui, T.H., Peng, Y., and Wing, B.A., 2018, Triple oxygen isotope evidence for limited mid-Proterozoic primary productivity: Nature, doi:10.1038/s41586-018-0349-y.

Dole, M., 1935, The relative atomic weight of oxygen in water and in air: Journal of the American Chemical Society, v. 57, p. 2731−2731.

Farquhar, J., Canfield, D.E., Masterson, A., Bao, H., and Johnston, D., 2008, Sulfur and oxygen isotope study of sulfate reduction in experiments with natural populations from Faellestrand, Denmark: Geochimica et Cosmochimica Acta, v. 72, p. 2805−2821.

Farquhar, J., and Wing, B.A., 2003, Multiple sulfur isotopes and the evolution of the atmosphere: Earth and Planetary Science Letters, v. 213, p. 1−13.

Gomes, M.L., and Johnston, D.T., 2017, Oxygen and sulfur isotopes in sulfate in modern euxinic systems with implications for evaluating the extent of euxinia in ancient oceans: Geochimica et Cosmochimica Acta, v. 205, p. 331−359, doi:10.1016/j.gca.2017.02.020.

Gonfiantini, R., Stichler, W., and Rozanski, K., 1995, Standards and intercomparison materials distributed by the International Atomic Energy Agency for stable isotope measurements: Reference and intercomparison materials for stable isotopes of light elements, TECDOC-825: International Atomic Energy Agency (1995), p. 13-29

Gregory, B.S., Claire, M.W., and Rugheimer, S., 2021, Photochemical modelling of atmospheric oxygen levels confirms two stable states: Earth and Planetary Science Letters, v. 561, p. 116818, doi:10.1016/j.epsl.2021.116818.

Gu, X., Heaney, P.J., Reis, F.D.A.A., and Brantley, S.L., 2020, Deep abiotic weathering of pyrite: Science, v. 370, doi:10.1126/science.abb8092.

Gumsley, A.P., Chamberlain, K.R., Bleeker, W., Söderlund, U., de Kock, M.O., Larsson, E.R., and Bekker, A., 2017, Timing and tempo of the Great Oxidation Event: Proceedings of the National Academy of Sciences, doi:10.1073/pnas.1608824114.

Hayles, J.A., Cao, X., and Bao, H., 2017, The statistical mechanical basis of the triple isotope fractionation relationship: Geochem. Perspect. Lett, v. 3, p. 1−11.

Heidel, C., and Tichomirowa, M., 2011, The isotopic composition of sulfate from anaerobic and low oxygen pyrite oxidation experiments with ferric iron—New insights into oxidation mechanisms: Chemical Geology, v. 281, p. 305−316.

Heidel, C., and Tichomirowa, M., 2010, The role of dissolved molecular oxygen in abiotic pyrite oxidation under acid pH conditions − Experiments with 18O-enriched molecular oxygen: Applied Geochemistry, v. 25, p. 1664−1675, doi:10.1016/j.apgeochem.2010.08.014.

Hemingway, J.D., Olson, H., Turchyn, A.V., Tipper, E.T., Bickle, M.J., and Johnston, D.T., 2020, Triple oxygen isotope insight into terrestrial pyrite oxidation: Proceedings of the National Academy of Sciences, v. 117, p. 7650−7657.

Hendry, M.J., Krouse, H.R., and Shakur, M.A., 1989, Interpretation of oxygen and sulfur isotopes from dissolved sulfates in tills of southern Alberta, Canada: Water Resources Research, v. 25, p. 567−572, doi:10.1029/WR025i003p00567.

Herwartz, D., Pack, A., Krylov, D., Xiao, Y., Muehlenbachs, K., Sengupta, S., and Di Rocco, T., 2015, Revealing the climate of snowball Earth from Δ17O systematics of hydrothermal rocks: Proceedings of the National Academy of Sciences, v. 112, p. 5337−5341, doi:10.1073/pnas.1422887112.

Hodgskiss, M.S.W., Crockford, P.W., Peng, Y., Wing, B.A., and Horner, T.J., 2019, A productivity collapse to end Earth's Great Oxidation: Proceedings of the National Academy of Sciences, v. 116, p. 17207−17212, doi:10.1073/pnas.1900325116.

Hoffman, P.F. et al., 2017, Snowball Earth climate dynamics and Cryogenian geology-geobiology: Science Advances, v. 3, doi:10.1126/sciadv.1600983.

Homann, M. et al., 2018, Microbial life and biogeochemical cycling on land 3,220 million years ago: Nature Geoscience, doi:10.1038/s41561-018-0190-9.

Johnson, A.C., Romaniello, S.J., Reinhard, C.T., Gregory, D.D., Garcia-Robledo, E., Peter Revsbech, N., Canfield, D.E., Lyons, T.W., and Anbar, A.D., 2019, Experimental

determination of pyrite and molybdenite oxidation kinetics at nanomolar oxygen concentrations: Geochimica et Cosmochimica Acta, doi:10.1016/j.gca.2019.01.022.

Kanzaki, Y., and Murakami, T., 2019, Rates and stoichiometry of pyrite dissolution at pH 3 under low O2 conditions: Chemical Geology, doi:10.1016/j.chemgeo.2019.05.009.

Killingsworth, B.A., Bao, H., and Kohl, I.E., 2018, Assessing Pyrite-Derived Sulfate in the Mississippi River with Four Years of Sulfur and Triple-Oxygen Isotope Data: Environmental Science & Technology, v. 52, p. 6126−6136, doi:10.1021/acs.est.7b05792.

Killingsworth, B.A., Sansjofre, P., Philippot, P., Cartigny, P., Thomazo, C., and Lalonde, S.V., 2019, Constraining the rise of oxygen with oxygen isotopes: Nature Communications, v. 10, p. 4924, doi:10.1038/s41467-019-12883-2.

Kim, Y., Lee, I., Seo, J.H., Lee, J.I., and Farquhar, J., 2017, Multiple oxygen (16O, 17O and 18O) and sulfur (32S, 33S, 34S and 36S) isotope signatures of the dissolved sulfate from Deception Island, Antarctic Peninsula: Implications on sulfate formation, transportation and deposition in the Antarctic region: Chemical Geology, doi:10.1016/j.chemgeo.2017.07.029.

Kipp, M.A., Krissansen-Totton, J., and Catling, D.C., 2021, High Organic Burial Efficiency Is Required to Explain Mass Balance in Earth's Early Carbon Cycle: Global Biogeochemical Cycles, doi: 10.1029/2020GB006707

Kohl, I., and Bao, H.M., 2011, Triple-oxygen-isotope determination of molecular oxygen incorporation in sulfate produced during abiotic pyrite oxidation (pH=2-11): Geochimica Et Cosmochimica Acta, v. 75, p. 1785−1798, doi:10.1016/j.gca.2011.01.003.

Krissansen-Totton, J., Buick, R., and Catling, D.C., 2015, A statistical analysis of the carbon isotope record from the Archean to Phanerozoic and implications for the rise of oxygen: American Journal of Science, v. 315, p. 275−316, doi:10.2475/04.2015.01.

Krouse, H.R., Gould, W.D., McCready, R.G.L., and Rajan, S., 1991, 18O incorporation into sulphate during the bacterial oxidation of sulphide minerals and the potential for oxygen isotope exchange between O2, H2O and oxidized sulphur intermediates: Earth and Planetary Science Letters, v. 107, p. 90−94, doi:10.1016/0012-821X(91)90045-J.

Kump, L.R., 2008, The rise of atmospheric oxygen: Nature, v. 451, p. 277−8, doi:10.1038/nature06587.

Landais, A., Lathiere, J., Barkan, E., Luz, B., 2007. Reconsidering the change in global biosphere productivity between the Last Glacial Maximum and present day from the triple oxygen isotopic composition of air trapped in ice cores. Global Biogeochemical Cycles 21 (GB1025). doi:10.1029/2006GB002739.

LeGendre, E., Martin, E., Villemant, B., Cartigny, P. and Assayag, N., 2017, A simple and reliable anion-exchange resin method for sulfate extraction and purification suitable for multiple O-and S-isotope measurements: Rapid Communications in Mass Spectrometry, v. 31, p.137-144, doi: 10.1002/rcm.7771

Lloyd, R., 1968, Oxygen isotope behavior in the sulfate-water system: Journal of Geophysical Research, v. 73, p. 6099−6110.

Luz, B., and Barkan, E., 2010, Variations of 17O/16O and 18O/16O in meteoric waters: Geochimica et Cosmochimica Acta, v. 74, p. 6276−6286, doi:10.1016/j.gca.2010.08.016.

Luz, B., Barkan, E., Bender, M.L., Thiemens, M.H., and Boering, K.A., 1999, Triple-isotope composition of atmospheric oxygen as a tracer of biosphere productivity: Nature, v. 400, p. 547−550.

Luz, B., Barkan, E., and Severinghaus, J.P., 2014, 5.14 - The Stable Isotopic Composition of Atmospheric O2, *in* Holland, H.D. and Turekian, K.K. eds., Treatise on Geochemistry (Second Edition), Oxford, Elsevier, p. 363−383, doi:10.1016/B978-0-08-095975-7.00419-8.

Martin, DMcB, 2020, Geology of the Hardey Syncline — the key to understanding the northern margin of the Capricorn Orogen: Geological Survey of Western Australia 203, 62 p.

Miller, M.F., Pack, A., Bindeman, I.N., and Greenwood, R.C., 2020, Standardizing the reporting of Δ′17O data from high precision oxygen triple-isotope ratio measurements of silicate rocks and minerals: Chemical Geology, v. 532, p. 119332.

Morita, N., 1935, The increased density of air oxygen relative to water oxygen: Journal of Chemical Society of Japan, v. 56, p. 1291.

Oba, Y., and Poulson, S.R., 2009, Oxygen isotope fractionation of dissolved oxygen during abiological reduction by aqueous sulfide: Chemical Geology, v. 268, p. 226−232, doi:10.1016/j.chemgeo.2009.09.002.

Pack, A., Höweling, A., Hezel, D.C., Stefanak, M.T., Beck, A.-K., Peters, S.T.M., Sengupta, S., Herwartz, D., and Folco, L., 2017, Tracing the oxygen isotope composition of the upper Earth's atmosphere using cosmic spherules: Nature Communications, v. 8, p. 15702, doi:10.1038/ncomms15702.

Pavlov, A., and Kasting, J., 2002, Mass-independent fractionation of sulfur isotopes in Archean sediments: strong evidence for an anoxic Archean atmosphere: Astrobiology, v. 2, p. 27−41.

Peng, Y., Bao, H., Zhou, C., Yuan, X., and Luo, T., 2013, Oxygen isotope composition of meltwater from a Neoproterozoic glaciation in South China: Geology, v. 41, p. 367−370, doi:10.1130/g33830.1.

Philippot, P. et al., 2018, Globally asynchronous sulphur isotope signals require re-definition of the Great Oxidation Event: Nature Communications, v. 9, p. 2245, doi:10.1038/s41467-018-04621-x.

Philippot, P., Killingsworth, B.A., Paquette, J.-L., Tessalina, S., Cartigny, P., Lalonde, S.V., Thomazo, C., Ávila, J.N., and Busigny, V., 2021, Comment on "Correlation of the stratigraphic cover of the Pilbara and Kaapvaal cratons recording the lead up to Paleoproterozoic Icehouse and the GOE" by Andrey Bekker, Bryan Krapež, and Juha A. Karhu, 2020, Earth Science Reviews, https://doi.org/10.1016/j.earscirev.2020.103389: Earth-Science Reviews, v. 218, p. 103594, doi:10.1016/j.earscirev.2021.103594.

Pierre, C., Ortlieb, L., and Person, A., 1984, Supratidal evaporitic dolomite at Ojo de Liebre Lagoon; mineralogical and isotopic arguments for primary crystallization: Journal of Sedimentary Research, v. 54, p. 1049−1061.

Planavsky, N.J., Reinhard, C.T., Isson, T.T., Ozaki, K., and Crockford, P.W., 2020, Large Mass-Independent Oxygen Isotope Fractionations in Mid-Proterozoic Sediments: Evidence for a Low-Oxygen Atmosphere? Astrobiology, v. 20, p. 628−636.

Poulton, S.W., Bekker, A., Cumming, V.M., Zerkle, A.L., Canfield, D.E., and Johnston, D.T., 2021, A 200-million-year delay in permanent atmospheric oxygenation: Nature, v. 592, p. 232−236, doi:10.1038/s41586-021-03393-7.

Prave, A.R., Kirsimae, K., Lepland, A., Fallick, A.E., Kreitsmann, T., Deines, Y.E., Romashkin, A.E., Rychanchik, D.V., Medvedev, P.V., Moussavou, M., Bakakas, K., and

Hodgskiss, M.S.W., 2021, The grandest of them all: the Lomagundi-Jatuli Event and Earth's oxygenation: Journal of the Geological Society, doi: 10.1144/jgs2021-036

Raymond, P.A., and Oh, N.-H., 2009, Long term changes of chemical weathering products in rivers heavily impacted from acid mine drainage: Insights on the impact of coal mining on regional and global carbon and sulfur budgets: Earth and Planetary Science Letters, v. 284, p. 50−56, doi:10.1016/j.epsl.2009.04.006.

Reinhard, C.T., Planavsky, N.J., and Lyons, T.W., 2013, Long-term sedimentary recycling of rare sulphur isotope anomalies: Nature, v. 497, p. 100−104.

Rimstidt, J.D., and Vaughan, D.J., 2003, Pyrite oxidation: a state-of-the-art assessment of the reaction mechanism: Geochimica et Cosmochimica Acta, v. 67, p. 873−880.

Seal, R.R., 2003, Stable-isotope geochemistry of mine waters and related solids: Environmental aspects of mine wastes, v. 31, p. 303−334.

Sengupta, S., Peters, S.T.M., Reitner, J., Duda, J.-P., and Pack, A., 2020, Triple oxygen isotopes of cherts through time: Chemical Geology, v. 554, p. 119789, doi:10.1016/j.chemgeo.2020.119789.

Shaheen, R., Janssen, C., and Rockmann, T., 2007, Investigations of the photochemical isotope equilibrium between O2, CO2 and O3: Atmos. Chem. Phys., p. 15.

Sun, T., Socki, R.A., Bish, D.L., Harvey, R.P., Bao, H., Niles, P.B., Cavicchioli, R., and Tonui, E., 2015, Lost cold Antarctic deserts inferred from unusual sulfate formation and isotope signatures: Nature communications, v. 6.

Taylor, B.E., and Wheeler, M.C., 1994, Sulfur- and Oxygen-Isotope Geochemistry of Acid Mine Drainage in the Western United States, *in* Environmental Geochemistry of Sulfide Oxidation, American Chemical Society, ACS Symposium Series, v. 550, p. 481−514, doi:10.1021/bk-1994-0550.ch030.

Taylor, B.E., Wheeler, M.C., and Nordstrom, D.K., 1984, Stable isotope geochemistry of acid mine drainage: Experimental oxidation of pyrite: Geochimica et Cosmochimica Acta, v. 48, p. 2669−2678.

Thiemens, M.H., 2006, History and applications of mass-independent isotope effects: Annual Review of Earth and Planetary Sciences, v. 34, p. 217−262, doi:10.1146/annurev.earth.34.031405.125026.

Thiemens, M.H., and Heidenreich, J.E., 1983, The mass-independent fractionation of oxygen: A novel isotope effect and its possible cosmochemical implications: Science, v. 219, p. 1073−1075.

Thiemens, M.H., Jackson, T., Mauersberger, K., Schueler, B. and Morton, J., 1991, Oxygen isotope fractionation in stratospheric CO2: Geophysical Research Letters, v. 18, p. 669-672, doi: 10.1029/91GL00121.

Thiemens, M.H., Jackson, T., Zipf, E.C., Erdman, P.W., and van Egmond, C., 1995, Carbon dioxide and oxygen isotope anomalies in the mesosphere and stratosphere: Science, v. 270, p. 969-972, doi: 10.1126/science.270.5238.969.

Thomazo, C., Couradeau, E., and Garcia-Pichel, F., 2018, Possible nitrogen fertilization of the early Earth Ocean by microbial continental ecosystems: Nature Communications, v. 9, p. 1-8, doi: 10.1038/s41467-018-04995-y.

Tichomirowa, M., and Junghans, M., 2009, Oxygen isotope evidence for sorption of molecular oxygen to pyrite surface sites and incorporation into sulfate in oxidation experiments: Applied Geochemistry, v. 24, p. 2072−2092.

Van Everdingen, Robert O., and Krouse, H.R., 1988, Interpretation of isotopic compositions of dissolved sulfates in acid mine drainage: U.S. Bureau of Mines Circular 9183: Mine Drainage and Surface Mine Reclamation, p. 147-156.

Van Kranendonk, M.J., Mazumder, R., Yamaguchi, K.E., Yamada, K., and Ikehara, M., 2015, Sedimentology of the Paleoproterozoic Kungarra Formation, Turee Creek Group, Western Australia: A conformable record of the transition from early to modern Earth: Precambrian Research, v. 256, p. 314−343.

Van Stempvoort, D., and Krouse, H., 1994, Controls of δ18O in sulfate: a review of experimental data and application to specific environments, C.N. Alpers, D.W. Blowes (Eds.), Environmental Geochemistry of Sulfide Oxidation. ACS Symposium Series. American Chemical Society (1994), p. 446-480 doi: 10.1021/bk-1994-0550.ch029

Waldeck, A.R., Cowie, B.R., Bertran, E., Wing, B.A., Halevy, I., and Johnston, D.T., 2019, Deciphering the atmospheric signal in marine sulfate oxygen isotope composition: Earth and Planetary Science Letters, v. 522, p. 12−19, doi:10.1016/j.epsl.2019.06.013.

Warke, M.R., Di Rocco, T., Zerkle, A.L., Lepland, A., Prave, A.R., Martin, A.P., Ueno, Y., Condon, D.J., and Claire, M.W., 2020, The Great Oxidation Event preceded a Paleoproterozoic "snowball Earth": Proceedings of the National Academy of Sciences,.

Wen, J., and Thiemens, M.H., 1993, Multi-isotope study of the O (1 D)+ CO2 exchange and stratospheric consequences: Journal of Geophysical Research: Atmospheres (1984−2012), v. 98, p. 12801−12808. doi: 10.1029/93JD00565

West, J.B., Sobek, A., and Ehleringer, J.R., 2008, A Simplified GIS Approach to Modeling Global Leaf Water Isoscapes: PLOS ONE, v. 3, p. e2447, doi:10.1371/journal.pone.0002447.

Williamson, M.A., and Rimstidt, J.D., 1994, The kinetics and electrochemical rate-determining step of aqueous pyrite oxidation: Geochimica et Cosmochimica Acta, v. 58, p. 5443−5454.

Yan, Y., Bender, M.L., Brook, E.J., Clifford, H.M., Kemeny, P.C., Kurbatov, A.V., Mackay, S., Mayewski, P.A., Ng, J., and Severinghaus, J.P., 2019, Two-million-year-old snapshots of atmospheric gases from Antarctic ice: Nature, v. 574, p. 663−666.

Young, E.D., Yeung, L.Y., and Kohl, I.E., 2014, On the Δ17O budget of atmospheric O2: Geochimica et Cosmochimica Acta, v. 135, p. 102−125, doi:10.1016/j.gca.2014.03.026.

Yung, Y.L., DeMore, W.B., and Pinto, J.P., 1991, Isotopic exchange between carbon dioxide and ozone via O (1D) in the stratosphere: Geophysical Research Letters, v. 18, p. 13−16.

Zhang, D., Zhao, Z., Li, X., Zhang, L., and Chen, A., 2020, Assessing the oxidative weathering of pyrite and its role in controlling atmospheric CO2 release in the eastern Qinghai-Tibet Plateau: Chemical Geology, v. 543, p. 119605, doi:10.1016/j.chemgeo.2020.119605.

SUPPLEMENTARY INFORMATION: Towards a holistic sulfate-water-O_2 triple oxygen isotope systematics

B.A. Killingsworth[a,b,*], P. Cartigny[c], J.A. Hayles[d], C. Thomazo[e,f], P. Sansjofre[b,1], V. Pasquier[g], S.V. Lalonde[b], and P. Philippot[c,h,i]

[a]United States Geological Survey, MS 954 National Center, 12201 Sunrise Valley Dr., Reston, Virginia 20192, USA
[b]CNRS-UMR6538 Laboratoire Géosciences Océan, European Institute for Marine Studies, Université de Bretagne Occidentale, 29280 Plouzané, France
[c]Institut de Physique du Globe de Paris, Sorbonne-Paris Cité, UMR 7154, CNRS-Université Paris Diderot, 75005 Paris Cedex 05, France
[d]Jacobs-JETS, Astromaterials Research and Exploration Science, Johnson Space Center, NASA, Houston, Texas 77058, USA
[e]UMR CNRS/uB 6282 Laboratoire Biogéosciences, Université de Bourgogne Franche-Comté, 6 Bd Gabriel, 21000 Dijon, France
[f]Institut Universitaire de France, 75005 Paris, France
[g]Department of Earth and Planetary Sciences, Weizmann Institute of Science, Rehovot 76100, Israel
[h]Géosciences Montpellier, CNRS-UMR 5243, Université de Montpellier, Montpellier Cedex 5, France
[i]Instituto de Astronomia, Geofísica e Ciências Atmosféricas, Universidade de São Paulo, Rua do Matão, 1226 - Cidade Universitária, 05508-090 São Paulo, Brazil
[*]correspondence to: bkillingsworth@usgs.gov
[1]current address: Muséum d'Histoire Naturelle, Sorbonne Université, UMR CNRS 7590, Institut de Minéralogie, de Physique des Matériaux et de Cosmochimie, 75005 Paris, France

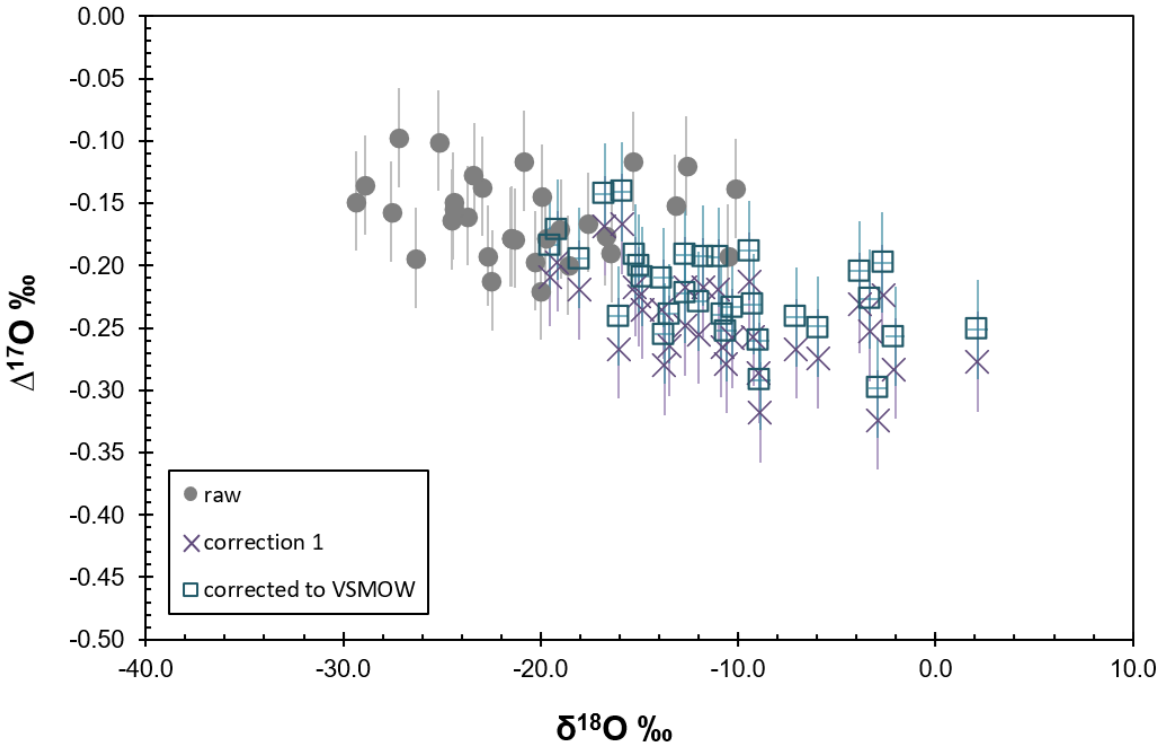

Figure S1. The normalization of Kazput barite triple oxygen isotope data ($\Delta^{17}O$ and $\delta^{18}O$) is shown, with 1) raw data (filled circles) that were measured at IPGP against an in-house reference O_2 gas, 2) the correction 1 data (x symbols) that are corrected for mass-dependent fractionation during partial sample yields during the CO_2-laser fluorination (using equation (13)), and 3) final normalization for the data to be corrected to the international standard VSMOW (open square symbols) (using equation (14)). Description of the normalization and its equations are found in the methods section 2.4 in the main text.

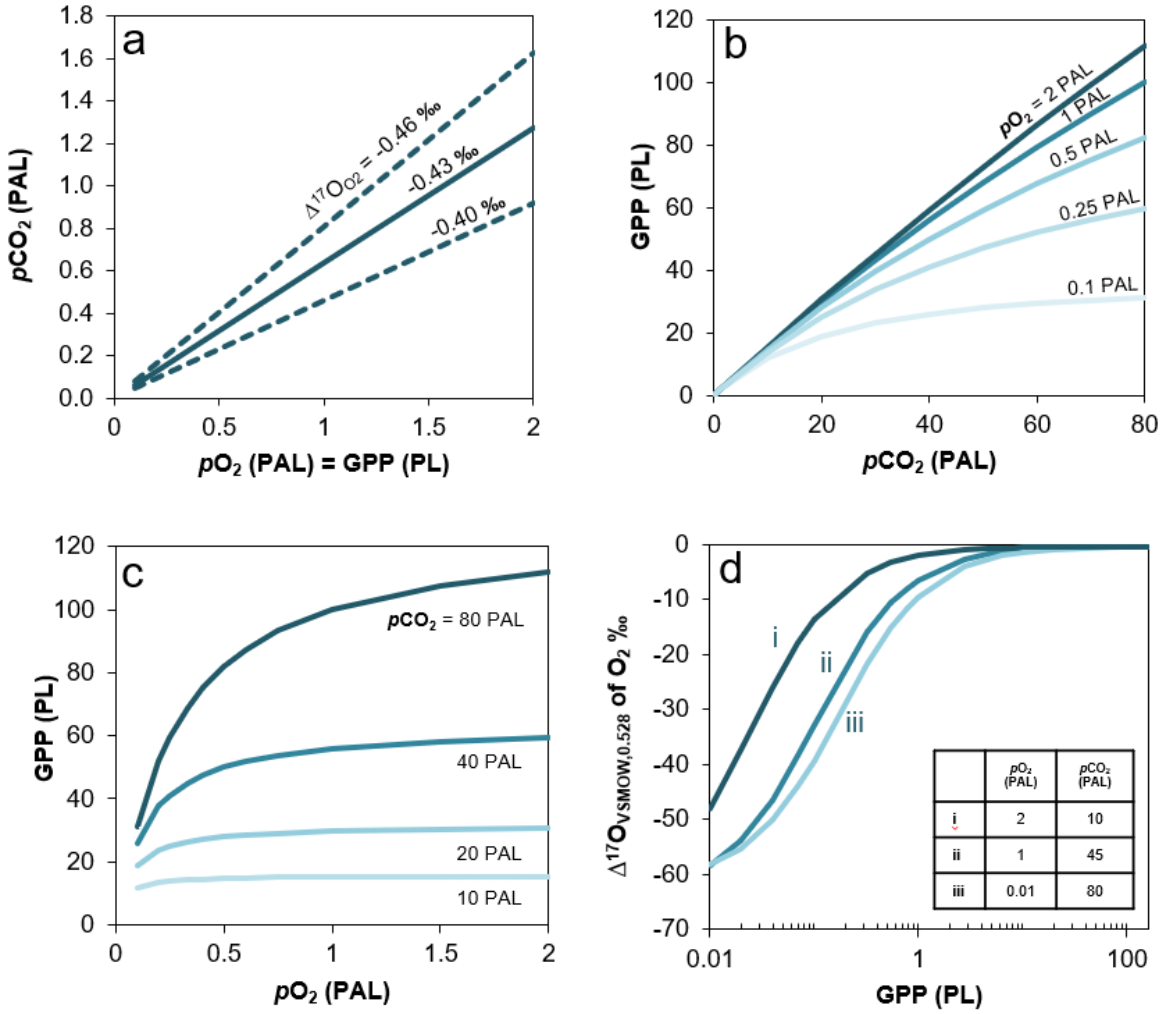

Figure S2. Four model sensitivity plots are shown that explore triple oxygen isotope constraints and estimates of atmospheric gas concentrations for the Paleoproterozoic, ca. 2.3 Ga. Plot (a) shows the resulting pCO_2 if pO_2 and gross primary productivity (GPP) were proportional, all within the ranges of Kazput barite-constrained $\Delta^{17}O_{O2}$. Such low pCO_2 estimates underscore that high GPP, and its decoupling from pO_2, must have been required to balance the high pCO_2 of 10 to 80 PAL (Crockford et al., 2019) estimated for the Paleoproterozoic. Plots (b) and (c) show GPP as a function of pCO_2 and pO_2, respectively, both with Kazput barite-constrained O_2 at $\Delta^{17}O_{VSMOW,0.528} = -0.43$ ‰. Plot (d) shows the $\Delta^{17}O_{VSMOW,0.528}$ of O_2 as a function of GPP under different combinations of pO_2 and pCO_2.

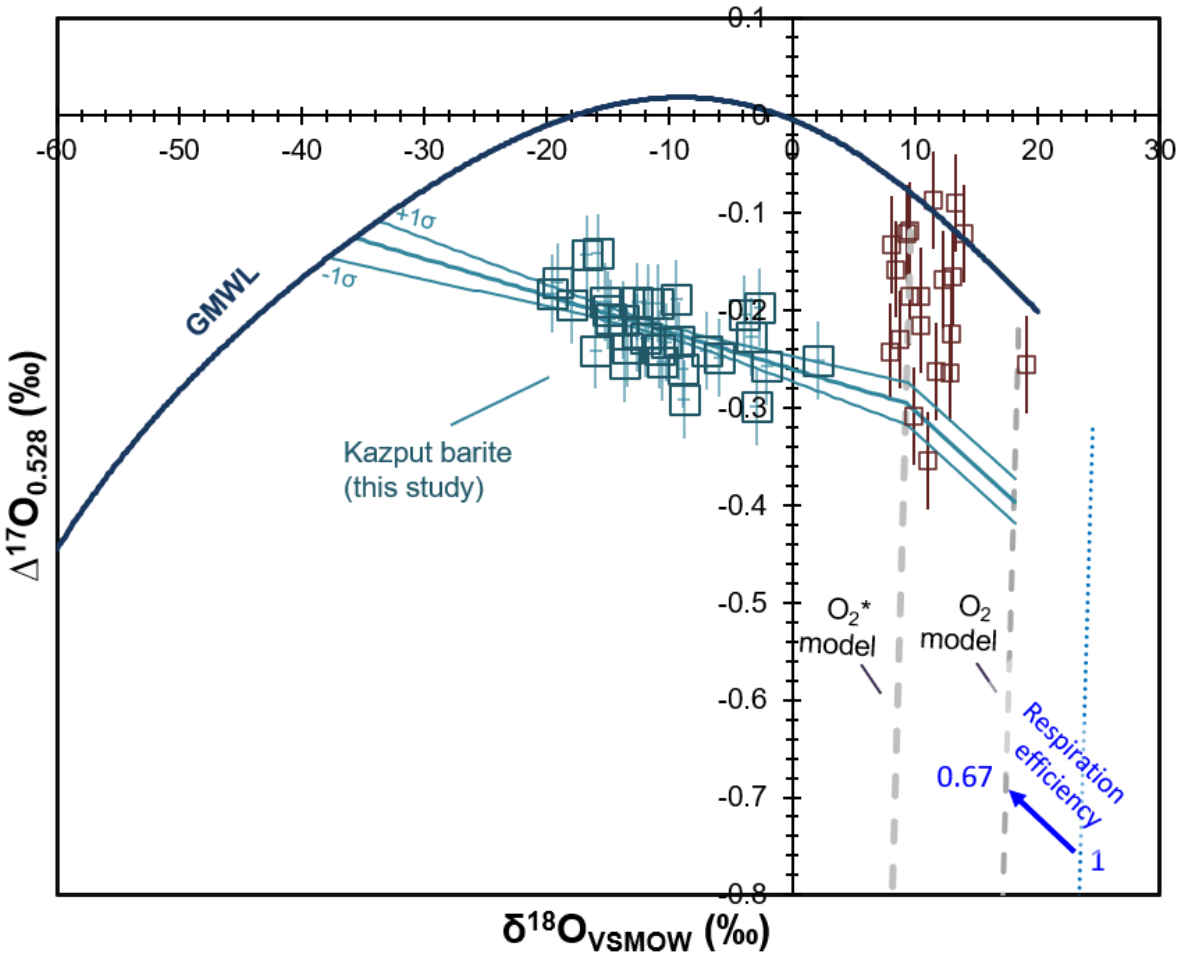

Figure S3. The effect on the O_2 model of changing respiration efficiency is shown. The O_2 model curve labeled 1 corresponds to modern-equivalent respiration efficiency, with a 0.67 fractional proportion of that moving the O_2 curve to its new labeled location. Triple oxygen isotope data of Kazput barite (large open squares; $\delta^{18}O$ from Killingsworth et al., 2019, and $\Delta^{17}O$ from this study) and Paleoproterozoic gypsum (small open squares; Crockford et al., 2019) are shown with the meteoric water line (MWL) and model O_2-oxygen curves, as described in the main text. Discussion of changing respiration efficiency is found in section 3.4 of the main text.